AIMS Mathematics, 10(10): 22929–22957.
DOI:10.3934/math.20251019
Received: 10 August 2025
Revised: 13 September 2025
Accepted: 24 September 2025
Published: 10 October 2025

https://www.aimspress.com/journal/Math

Research article

Chaos, Lyapunov exponent, and sensitivity demonstration of the coupled nonlinear integrable model with soliton solutions

Khizar Farooq[1], **Aljethi Reem Abdullah**[2], **Ejaz Hussain**[3,*] **and Muhammad Amin S. Murad**[4]

[1] Centre for High Energy Physics, University of the Punjab, Quaid-e-Azam Campus, Lahore 54590, Pakistan

[2] Department of mathematics and statistics, college of science, Imam Mohammad Ibn Saud Islamic University (IMSIU), Riyadh, Saudi Arabia

[3] Department of Mathematics, University of the Punjab, Quaid-e-Azam Campus, Lahore-54590, Pakistan

[4] Department of Cybersecurity, College of Engineering Technology, Alnoor University, Mosul 41012, Iraq

* **Correspondence:** Email: ejz.math@gmail.com

Abstract: The stochastic Schrödinger–Hirota equation is a well-established model for describing nonlinear pulse propagation in magneto-optic waveguides and fiber optics. While prior research has primarily concentrated on isolated soliton solutions, broader chaotic dynamics affecting signal stability remain less explored. In this work, we applied the Generalized Arnous method, planar dynamical system theory, and numerical simulations with the Runge–Kutta method to construct and analyze the solutions of the stochastic Schrödinger–Hirota equation. The result yielded tan-type bright, cot-type dark, and periodic solutions. Chaotic behavior was characterized via bifurcation diagrams, positive Lyapunov exponents, Poincaré sections, and time-series analyses. Sensitivity to initial conditions confirmed the presence of deterministic chaos. These results demonstrate that the stochastic Schrödinger–Hirota equation displays a rich spectrum of dynamical behavior, with the stability strongly influenced by parameter variations and perturbations. These insights offer a theoretical foundation for advancing the stability of optical soliton transmission and reducing the adverse effects of chaos in nonlinear communication systems.

Keywords: the generalized stochastic Schödinger-Hirota equation; generalized Arnous method; chaotic phenomena; bifurcation analysis; multistability; Lyapunov exponents; sensitivity analysis
Mathematics Subject Classification: 26A48, 26A51, 33B10, 37K40, 39B62

1. Introduction

Researchers hope to understand the complexities of nature. Partial differential equations (PDEs) are valuable tools for modeling complex phenomena. Among them, nonlinear partial differential equations (NLPDEs) are very important in solving physical problems. NLPDEs provide valuable insights into a variety of fields, helping scientists make accurate predictions about behavior and evolution. Advances in 3D visualization have enhanced their analytical capabilities. Many researchers are now focusing on NLPDE to better understand the structure of the universe.

A soliton is a self-reinforcing wave that maintains its shape as it propagates. It appears in inhomogeneous systems in response to other NLPDEs. Unlike normal waves, which disperse and spread out over time, single-mode waves remain unchanged as they propagate and do not spread out. Solitary waves play a key role in several scientific and technical sectors owing to their unusual ability to keep their form and speed across vast distances and via interactions. In physics [1] and engineering [2], solitons are used to simulate stable wave phenomena in nonlinear optics [3], fluid dynamics [4], and plasma physics [5], such as optical pulses in fiber optics [6] and ion-acoustic waves in space plasmas. They are also significant in biological [7] systems for understanding nerve signal transmission and pattern generation, and in chemistry [8] for characterizing reaction-diffusion processes. In mathematics [9], solitons give insight into nonlinear dynamics [10], chaos theory [11], and integrable systems. Their stability and resilience make them important for applications in electronics [12], telecommunications, and maybe even in quantum computing [13], giving solutions for signal processing, data transfer, and stable information storage.

Studying the single-wave solutions of NLPDEs is crucial for generating improved insights and knowledge of their underlying mechanism and valuable usage. Therefore, various academics have established novel approaches to investigate these NLPDE solutions. Plenty of strong techniques are available such as the $\exp(-\chi(\Theta))$ expansion method [14], extend mapping method [15], GAE scheme [16], homotopy perturbation method [17], Darboux transformation [18], generalized Kudryashov method [19], extended trial equation method [20], Hirota bilinear method [21], polynomial complete discriminant method [22], extended Jacobian method [23], extended direct algebraic method [24], modified sub-equation method [25], improved extended fan-sub equation method [26], modified extended tanh method, Bäcklund transform method [27], extended $(\frac{G'}{G})$ expansion method [28], extended auxiliary equation mapping method [29], IBSEF method [30], extended simple equation method [31], and new Kudryashov method [32].

Nonlinear partial differential equations (NLPDEs) are important tools in scientific studies, offering useful insights into fields such as plasma, dynamics, acoustics, optics, and condensed matter physics. These equations not only help in our comprehension of complicated behaviors but also allow scientists to make exact predictions regarding their future growth. Consequently, many scholars are investigating a range of NLPDEs to better understand complicated behaviors in natural systems. Recent studies have examined equations such as the Schrödinger equation [33, 34], Batman-Burger equation [35], Benjamin-Bona-Mahony equation [36], generalized Calogero-Bogoyavlenskii-Schiff equation [37], Date-Jimbo-Kashiwara-Miwa equation [38], thin film ferroelectric material equation [39], Boussinesq equation [40], and nonlinear non-classical Sobolev-type wave model [41].

Bifurcation analysis [42] is a fundamental tool to analyze nonlinear systems. It provides insight into the nature of the system's behavior variation with respect to parameters. Detection of bifurcation

points by a quantitative transformation of the dynamics of the system allows to predict and investigate the transitions between the states of equilibrium, periodic solutions, and chaotic activity. In addition to regular soliton propagation, nonlinear wave models such as the Schrödinger–Hirota equation can exhibit chaotic dynamics under perturbations. Studying chaos is significant because it reveals the parameter regimes where stable pulse transmission is lost, leading to irregular oscillations or signal degradation in optical and plasma systems. Thus, analyzing chaotic responses through tools like bifurcation diagrams, Lyapunov exponents, and Poincaré maps provides both theoretical insight and practical guidance for controlling nonlinear wave behavior in realistic environments. The quantitative measure of sensitivity is through the Lyapunov exponent, which computes the rate at which the trajectories diverge from each other. A positive Lyapunov exponent indicates that the system is chaotic. Bifurcation analysis is closely related to modulation stability, which looks at the stability of wave patterns against disturbances. The study of how waves behave when subjected to small perturbations may be crucial in explaining the development of instabilities that may eventually give rise to phenomena such as rogue waves in optical systems or turbulence in fluids. Such analysis is quite crucial in engineering and control systems, as appropriate parameter settings could avoid catastrophes or enhance performance.

Practical applications of bifurcation analysis [43] are extensive. It is used in designing stable chemical reactors, understanding population dynamics in ecological models, and ensuring stability in electric circuits. This ability to map out bifurcation diagrams provides a clear visual representation of stable and unstable regions, aiding in decision-making and system design.

1.1. Formulation of model

This work examines the stochastic Schrödinger–Hirota equation (SSHE) in magneto-optic waveguides, expressed as.

$$\left.\begin{aligned} &i\mathfrak{Q}_t + j_1\mathfrak{Q}_{xx} + (k_1|\mathfrak{Q}|^{2n} + l_1|\varphi|^{2n})\mathfrak{Q} + id_1\mathfrak{Q}_{xxx} + i(m_1|\mathfrak{Q}|^{2n} + n_1|\varphi|^{2n})\mathfrak{Q}_x + \epsilon\mathfrak{Q}\frac{dZ}{dt} \\ &= P_1\varphi + i[s_1\varphi_x + \alpha_1(|\varphi|^{2n}\varphi)_x + \nu_1(|\varphi|^{2n})_x\varphi], \\ &i\mathfrak{Q}_t + j_2\mathfrak{Q}_{xx} + \left(k_2|\mathfrak{Q}|^2 n + l_2|\mathfrak{Q}|^2 n\right)\mathfrak{Q} + id_2\mathfrak{Q}_{xxx} + i\left(m_2|\mathfrak{Q}|^2 n + n_2|\mathfrak{Q}|^2 n\right)\mathfrak{Q}_x + \epsilon\mathfrak{Q}\frac{dZ}{dt} = \\ &P_2\varphi + i\left[s_2\varphi_x + \alpha_2\left(|\varphi|^2 n\varphi\right)_x + \nu_2\left(|\varphi|^2 n\right)_x\varphi\right]. \end{aligned}\right\} \tag{1.1}$$

The complex functions $\mathfrak{Q}(x,t)$ and $\varphi(x,t)$ present a wave profile. The constants a_c (c = 1,2) correspond to chromatic dispersion (CD) coefficients. Self-phase modulation and cross-phase modulation (XPM) are represented by k_c and l_c (c = 1,2), respectively. Third-order dispersion (3OD) is described by d_c (c =1,2). The coefficients M_c and n_c (c = 1,2) account for nonlinear effects. The noise strength coefficient is ϵ, and Z(t) denotes the standard Wiener process, with $\frac{dZ}{dt}$ indicating white noise. Magneto-optic waveguide terms are expressed as P_c (c = 1,2). Finally, s_c, ν_c, and α_c (c = 1,2) represent inter-model dispersion (IMD), nonlinear dispersion, and self-steepening (SS) coefficients, respectively.

The generalized SSHE in magneto-optic waveguides is a classical model with applications across various fields, including chemical circulation systems, heat pulses in solids, nonlinear optics, fluid mechanics, ecology, optical fiber in communication, plasma physics, and engineering.

1.2. Literature review

Many scholars and researchers have focused on developing traveling wave solutions and optical solitons for this model. Zayad et al. [44] used the extended simplest equation algorithm to derive optical solitons for the system (1.1). Additionally, Zayed et al. [45] obtained new optical solutions and solutions in terms of Jacobi's elliptic using the Φ_6 expansion scheme method. Tang et al. [46] obtained the optical traveling soliton solutions in magneto-optic waveguides. Cakicioglu et al. [47] derived the optical solitons of Schrödinger–Hirota equation with parabolic-law nonlinearity via generalized Kudryashov algorithm, illustrating its capability to produce exact analytical solutions for this class of nonlinear wave models. Kumar et al. [48] derived the diverse optical solitons and soliton-like solutions of the Schrödinger–Hirota equation with parabolic-law nonlinearity using the modified generalized Riccati-equation mapping approach. Biswas et al. [49] obtained optical soliton solutions for the Schrödinger–Hirota equation in a power-law medium via the G'/G-expansion approach, representing the effectiveness of the method in handling nonlinearity beyond Kerr law models. Kilic et al. [50] derived optical soliton solutions of the Schrödinger–Hirota equation with power-law nonlinearity by applying the Bäcklund transformation. Han et al. [51] analyzed dynamics of perturbed Schrödinger–Hirota equation with cubic–quintic–septic nonlinearity in dispersive media, and reported a variety of soliton solutions under higher-order nonlinear effects. Novel expansion and auxiliary-equation schemes have been used recently to construct new traveling-wave, kink, and lump solutions of (2+1)-dimension Hirota–Satsuma–Ito–type equations [52]. Han et al. [53] investigated the nonlinear dissipative (2+1)-dimensional model and constructed high-order solitary waves, fission structures, hybrid waves, and various interaction solutions.

1.3. Research aim and objectives

This study examines the SSHE as a fundamental model for nonlinear wave propagation in magneto-optic waveguides and fiber optics, emphasizing soliton solutions and chaotic dynamics. Exact solutions of SSHE are derived using the generalized Arnous method, and their dynamical properties are analyzed employing planar dynamical theory. This analysis yields distinct solution families, including bright solitons, dark solitons, and periodic waves, each systematically characterized. Numerical simulations based on the Runge-Kutta method are employed to investigate bifurcation diagrams, Lyapunov exponents, Poincaré sections, and time-series responses, revealing quasi-periodicity and chaotic regimes. This integrated analytical and numerical approach clarifies how the parameter variations and perturbations elucidate the sensitivity of the soliton stability, providing insight relevant to optical communication and chaotic phenomena in nonlinear media.

1.4. Contribution and originality

This research undertakes a detailed study of SSHE, focusing on both exact wave solutions and dynamical features of nonlinear systems. Using the traveling wave transformation together with the generalized Arnous method, an extensive class of exact solutions is obtained, including trigonometric, exponential, and soliton types, supported with two- and three-dimensional graphical representations. The originality of this study lies in its integration of bifurcation theory, chaotic dynamics, multi-stability, Lyapunov exponents, and sensitivity analysis to explore the stability and nonlinear transitions in a unified framework. Distinct from the earlier studies restricted to deterministic models or limited

solution families, this research considers the stochastic perturbations and external forcing, revealing a rich spectrum of dynamical phenomena such as quasi-periodicity, chaos, and the coexistence of multiple attractors. The contribution is twofold: mathematically, it extends the SSHE solution space with exact solitary waves; from the physical standpoint, it offers a deeper understanding of nonlinear interactions, modulation stability, and sensitivity in optical fibers, plasma, fluid dynamics, and magneto-optic waveguides. Collectively, these outcomes advance the theoretical foundation of SSHE and highlight new opportunities in stable transmission, chaos control, and nonlinear engineering systems.

The article is summarized as follows: Section 2 outlines the mathematical analysis required to transform the nonlinear partial differential problem into an ordinary differential equation. Section 3 examines the generalized Arnous method and its applications, with graphical representations. Section 4 highlights bifurcation analysis, chaotic behavior, multistability, Lyapunov exponent, and sensitivity analysis of our model. In Section 5, we discuss the graphical description and application of the obtained solutions and dynamical analysis. In Table 1, we discuss the comparison of the literature of Eq (1.1). In Table 2, we add the nomenclature of this article. Section 6 concludes our study.

Table 1. Comparison of literature on soliton solutions of the Schrödinger–Hirota equation.

Reference	**Methodology used**	**Main outcomes/solutions**
Zayed et al. [44]	Extended simplest equation method	Optical soliton solutions for system (1.1)
Zayed et al. [45]	Φ^6-expansion scheme	Optical solitons and Jacobi elliptic solutions
Tang et al. [46]	Analytical construction	Optical traveling solitons in magneto-optic waveguides
Cakicioglu et al. [47]	Generalized Kudryashov algorithm	Solitons with parabolic-law nonlinearity
Kumar et al. [48]	Modified Riccati-equation mapping	Optical soliton-like solutions under parabolic law
Biswas et al. [49]	G'/G-expansion method	Solitons in power-law medium, beyond Kerr-law
Kilic et al. [50]	Bäcklund transformation	Optical solitons with power-law nonlinearity
Han et al. [51]	Cubic–quintic–septic model	Soliton families in dispersive nonlinear media
Han et al. [53]	Auxiliary-equation schemes	High-order solitary waves, fission, hybrid solutions
GA method + dynamical analysis	GA method combined with bifurcation and chaos theory	Novel kink, bright, dark, and rational solitons (new type); analysis of bifurcation, multistability, chaos, Lyapunov exponents, and sensitivity under stochastic perturbations

Table 2. Nomenclature of parameters and variables used in this study.

Symbol	Description/physical meaning
x	Spatial coordinate
t	Temporal coordinate
$\xi = x - \omega_0 t$	Traveling-wave variable (co-moving frame)
$u(t, x), v(t, x)$	Field variables / wave components of the coupled system
$\phi(t, x)$	Second field in the coupled model
B	Amplitude-related parameter in the generalized Arnous method
H	Scaling constant in logarithmic solution form
η	Nonlinear phase or coupling parameter in solution ansatz
δ	Solution-shaping parameter (affects exponential/hyperbolic parts)
ν	Nonlinearity index controlling wave steepness
n_1	Coefficient in nonlinear interaction term
k_1	Nonlinear coupling strength parameter
d_1	Dispersion coefficient (controls soliton width)
A, P	Amplitude and phase constants in solution structure
s_1, l_1	Solution constants controlling wave symmetry and profile
m_1	Coefficient linked to higher-order nonlinearity
α_1	Fractional-order or scaling parameter in reduced ODE
λ	Auxiliary integration constant from solution process
ω_0	Soliton velocity (propagation speed of traveling wave)
ϵ	Noise intensity (strength of stochastic perturbation)
$Z(t)$	Wiener process (standard Brownian motion)
Lyapunov exponent (Λ)	Stability indicator: $\Lambda < 0$ (stable), $\Lambda > 0$ (chaotic)
Multistability	Existence of multiple stable states under the same parameters
Bifurcation	Parameter-driven change in solution stability/structure

2. Mathematical investigation

The generalized NLPDE can be expressed in the following form:

$$\mathfrak{Q}(\mathfrak{Q}, \mathfrak{Q}_t, \mathfrak{Q}_x, \mathfrak{Q}_y, \mathfrak{Q}_z, \mathfrak{Q}_{t,t}, \mathfrak{Q}_{x,x}, ...) = 0. \tag{2.1}$$

While the function $\mathfrak{Q} = \mathfrak{Q}(t, y, x)$ is still not known, by applying the below transformation, we can convert the NPLDE as shown in Eq (1.1) into an ODE.

$$\left.\begin{aligned} \mathfrak{Q}(t, x) &= \Re_1(\xi) \exp\left(-\nu x + \mu t + \epsilon Z(t) - \epsilon^2 t\right), \\ \varphi(t, x) &= \Re_2(\xi) \exp\left(-\nu x + \mu t + \epsilon Z(t) - \epsilon^2 t\right) \end{aligned}\right\}. \tag{2.2}$$

and,

$$\xi = x - \omega_0 t. \tag{2.3}$$

The non-zero real constants ν, ω_0, and μ represent the frequency, velocity, and wave number of the soliton, respectively. The functions $\Re_1(\xi)$ and $\Re_2(\xi)$ are real functions that describe the amplitude portion of solitons. The multiplicative stochastic factor in Eq (2.2) is

$$M_t = \exp(\epsilon Z(t) - \epsilon^2 t),$$

where $Z(t)$ denotes the standard Wiener process. By Itô's formula, one has

$$dM_t = M_t(\epsilon\, dZ_t - \tfrac{1}{2}\epsilon^2\, dt).$$

Writing

$$\phi(t, x) = R_1(\xi)\, e^{-\nu x+\mu t}\, M_t, \qquad \xi = x - \omega_0 t,$$

and applying the Itô product rule yields

$$d\phi = \phi(\epsilon\, dZ_t - \tfrac{1}{2}\epsilon^2\, dt) - \omega_0\, e^{-\nu x+\mu t} M_t R_1'(\xi)\, dt.$$

The original stochastic PDE (1.1) already contains the forcing term $\epsilon\phi\, dZ_t$. Substituting the above expression for $d\phi$ shows that the dZ_t–dependent pieces coming from dQ and from the explicit noise term have the same multiplicative structure, and thus are absorbed when the real and imaginary parts are separated. The remaining Itô drift term $-\frac{1}{2}\epsilon^2$ is deterministic and is incorporated into the coefficients (e.g., into μ or the combination written as $-\epsilon^2$ in Eq (2.2)). Consequently, the reduced profile equations for $R_1(\xi)$ and $R_2(\xi)$ are purely deterministic ordinary differential equations.

By substituting Eqs (2.2) and (2.3) into Eq (1.1), we can separately extract the real and imaginary parts of the equation.

$$(j_1+3d_1\nu)\Re_1'' - (\nu-\epsilon^2+j_1\nu^2+n_1\nu^3+s_1\nu)\Re_1 + (k_1+m_1\nu-\alpha_2\nu)\Re_1^{2n+1} + (l_1+n_1\nu)\Re_1\Re_2^{2n} + P_1\Re_2 = 0 \tag{2.4}$$

and,

$$(j_2+3d_2\nu)\Re_2'' - (\nu-\epsilon^2+j_2\nu^2+n_2\nu^3+s_2\nu)\Re_2 + (k_2+m_2\nu-\alpha_2\nu)\Re_2^{2n+1} + (l_2+n_2\nu)\Re_2\Re_1^{2n} - P_2\Re_1 = 0, \tag{2.5}$$

and the imaginary parts are

$$d_1\Re_1''' - (\omega_0 + 2j_1\nu + 3n_1\nu^2 + s_1)\Re_1' + [m_1 - 2n\nu_1 - (2n+1)\alpha_1]\,\Re_1^{2n}\Re_1' + n_1\Re_2^{2n}\Re_1' = 0 \tag{2.6}$$

and,

$$d_2\Re_2''' - (\omega_0 + 2j_2\nu + 3n_2\nu^2 + s_2)\Re_2' + [m_2 - 2n\nu_2 - (2n+1)\alpha_2]\,\Re_2^{2n} + \Re_2' + n_2\Re_1^{2n}\Re_2' = 0. \tag{2.7}$$

Assume a linear relationship exists between $\Re_1$ and $\Re_2$ such that $\Re_2 = A\Re_1$ where $(A \neq 0)$. Substituting $\Re_2 = A\Re_1$ in Eq (2.4) to Eq (2.7), we obtain:

$$(j_1+3d_1\nu)\Re_1'' - (\mu-\epsilon^2+j_1\nu^2+d_1\nu^3+s_1\nu+AP_1)\Re_1 + \left[k_1+m_1\nu-\alpha_1\nu(l_1+n_1\nu)A^{2n}\right]\Re_1^{2n+1} = 0, \tag{2.8}$$

$$(j_2 + 3d_2\nu)\Re_1'' - (\mu - \epsilon^2 + j_2\nu^2 + d_2\nu^3 + s_2\nu + AP_2)\Re_1 + \left[k_2 + m_2\nu - \alpha_2\nu(l_2 + n_2\nu)A^{2n}\right]\Re_1^{2n+1} = 0, \quad (2.9)$$

and

$$d_1\Re_1''' - (\omega_0 + 2j_1\nu + 3d_1\nu^2 + s_1)\Re_1' + \left[m_1 - 2nv_1 - (2n+1)\alpha_1 + n_1A^{2n}\right]\Re_1^{2n}\Re_1' = 0, \quad (2.10)$$

$$d_1\Re_1''' - (\omega_0 + 2j_2\nu + 3d_2\nu^2 + s_2)\Re_1' + \left[n_2 + A^{2n}(m_2 - 2nv_2 - (2n+1)\alpha_2)\right]\Re_1^{2n}\Re_1' = 0. \quad (2.11)$$

By integrating Eq (2.10) and Eq (2.11),

$$d_1\Re_1'' - (\omega_0 + 2j_1\nu + 3d_1\nu^2 + s_1)\Re_1 + \frac{1}{2n+1}\left[m_1 - 2nv_1 - (2n+1)\alpha_1 + n_1A^{2n}\right]\Re_1^{2n+1} = 0, \quad (2.12)$$

$$d_2\Re_1'' - (\omega_0 + 2j_2\nu + 3d_2\nu^2 + s_2)\Re_1 + \frac{1}{2n+1}\left[n_2 + A^{2n}(m_2 - 2nv_2 - (2n+1)\alpha_2)\right]\Re_1^{2n}\Re_1' = 0. \quad (2.13)$$

According to Eq (2.12) and Eq (2.13), we have

$$\frac{d_1}{d_2} = \frac{\omega_0 + 2j_1\nu + 3d_1\nu^2 + s_1}{\omega_0 + 2j_2\nu + 3d_2\nu^2 + s_2} = \frac{m_1 - 2nv_1 - (2n+1)\alpha_1 + n_1A^{2n}}{n_2 + A^{2n}(m_2 - 2nv_2 - (2n+1)\alpha_2)}. \quad (2.14)$$

We can find the velocity of the soliton from Eq (2.14) as:

$$\omega_0 = \frac{2(j_1d_2 - j_2d_1)\nu - s_2d_1 + s_1d_2}{d_1 - d_2}, \quad (d_1 \neq d_2). \quad (2.15)$$

Let n =1 for Eq (2.8), we obtain:

$$\Re_1'' + \frac{k_1 + m_1\nu - \alpha_1\nu(l_1 + n_1\nu)A^2}{j_1 + 3d_1\nu}\Re_1^3 - \frac{\lambda - \epsilon^2 + j_1\nu^2 + d_1\nu^3 + s_1\nu + AP}{j_1 + 3d_1\nu}\Re_1 = 0. \quad (2.16)$$

We will now focus on obtaining new traveling waves and optical solitons for the SSHE. This will be achieved using the complete discriminant model system and symbolic computation.

3. Generalized Arnous method

The basic steps of the generalized Arnous (GA) method are as follows [54]:
Step 01: The GA method provides the solution of Eq (2.16) as follows:

$$\Im(\xi) = a_0 + \sum_{i=1}^{N} \frac{a_i + b_i\Omega'(\xi)^i}{\Omega(\xi)^i}. \quad (3.1)$$

where a_0, a_i, b_i (for i = 1, 2, . . . , N) are constants, and the function $\Omega(\xi)$ verifies the relation

$$[\Omega'(\xi)]^2 = [\Omega(\xi)^2 - \eta]\ln[B], \quad (3.2)$$

with

$$\Omega^{(n)}(\xi) = \begin{cases} \Omega(\xi)\ln(B)^n, & \text{if } n \text{ is even,} \\ \Omega'(\xi)\ln(B)^{n-1}, & \text{if } n \text{ is odd,} \end{cases} \quad (3.3)$$

where $n \geq 2$, and $B \neq 1$. Eq (3.2) has solutions of the form:

$$\mathfrak{Q}(\xi) = H\ln(B)B^{\xi} + \frac{\eta}{4H\ln(B)B^{\xi}}. \tag{3.4}$$

where β and ϵ are arbitrary parameters.

Step 02: By balancing the nonlinear term and the term with the highest order derivative in Eq (2.3), the positive integer N is determined for Eq (3.1).

Step 03: After inserting Eq (3.2) and Eq (3.5) in Eq (2.16) and since $\mathfrak{Q}(\xi) = 0$, as a result of this substitution, we get a polynomial of $\frac{1}{\mathfrak{Q}(\xi)}\left(\frac{\mathfrak{Q}'(\xi)}{\mathfrak{Q}(\xi)}\right)$. Equivalently, setting all terms with the same power equal to zero, and by solving this set of nonlinear algebraic systems and with the help of Eq (3.2) and Eq (2.2), the solutions of Eq (1.1) may be determined.

3.1. Solitary wave solution by generalized Arnous method

To find the exact solution of Eq (2.3), first we find the value of positive integer $N = 1$; plugging the value of N in Eq (3.1), then Eq (3.1) will become as follows:

$$\mathfrak{F}(\xi) = a_0 + \frac{a_1}{\mathfrak{Q}(\xi)} + \frac{b_1\mathfrak{Q}'(\xi)}{\mathfrak{Q}(\xi)}. \tag{3.5}$$

By inserting Eq (3.5) into Eq (2.3), together with Eq (2.3) and Eq (3.2), we have a polynomial in terms of $\frac{1}{\mathfrak{L}}\left(\frac{L'(\xi)}{\mathfrak{L}}\right)$. This creates a system of algebraic equations when we aggregate all terms of the same power and set them to zero. The values of unknown constants are obtained.

Set 01.

$$\begin{aligned} a_0 &= -\frac{\log(\delta)\sqrt{AP - 2d_1\nu^3 + \lambda + \nu s_1 - \epsilon^2}}{\sqrt{\left(\log^2(\delta) + 2\nu^2\right)\left(\nu\left(m_1 - \alpha_1 A^2\left(l_1 + \nu n_1\right)\right) + k_1\right)}}, a_1 = 0, B = 1, \\ j_1 &= -\frac{2\left(AP + \lambda + \nu s_1 - \epsilon^2\right) + d_1\left(3\nu\log^2(\delta) + 2\nu^3\right)}{\log^2(\delta) + 2\nu^2}. \end{aligned} \tag{3.6}$$

By putting set 1 in Eq (3.5), we obtain the exact solution as follows:

$$\mathfrak{Q}_1(\xi) = \frac{b_1\left(HB^{\xi}\log^2(B) - \frac{\eta B^{-\xi}}{4H}\right)}{\frac{\eta B^{-\xi}}{4H\log(B)} + HB^{\xi}\log(B)} - \frac{\log(\delta)\sqrt{AP - 2d_1\nu^3 + \lambda + \nu s_1 - \epsilon^2}}{\sqrt{\left(\log^2(\delta) + 2\nu^2\right)\left(\nu\left(m_1 - \alpha_1 A^2\left(l_1 + \nu n_1\right)\right) + k_1\right)}}. \tag{3.7}$$

When we choose B = e and $\eta = 4H^2$, the Eq (3.7) is

$$\mathfrak{Q}_2(\xi) = b_1\tanh(x - t\omega_0) - \frac{\log(\delta)\sqrt{AP - 2d_1\nu^3 + \lambda + \nu s_1 - \epsilon^2}}{\sqrt{\left(\log^2(\delta) + 2\nu^2\right)\left(\nu\left(m_1 - \alpha_1 A^2\left(l_1 + \nu n_1\right)\right) + k_1\right)}}. \tag{3.8}$$

When we choose B = e and $\eta = -4H^2$, the Eq (3.7) is

$$\mathfrak{Q}_3(\xi) = b_1\coth(x - t\omega_0) - \frac{\log(\delta)\sqrt{AP - 2d_1\nu^3 + \lambda + \nu s_1 - \epsilon^2}}{\sqrt{\left(\log^2(\delta) + 2\nu^2\right)\left(\alpha_1 A^2 l_1(-\nu) - \alpha_1 A^2\nu^2 n_1 + k_1 + \nu m_1\right)}}. \tag{3.9}$$

Set 02.

$$a_0 = 0, a_1 = \frac{\sqrt{2}\,\sqrt{\eta}\log(\delta)\sqrt{AP - 2d_1\nu^3 + \lambda + \nu s_1 - \epsilon^2}}{\sqrt{\left(\log^2(\delta) - 2\nu^2\right)\left(\nu\left(m_1 - \alpha_1 A^2\left(l_1 + \nu n_1\right)\right) + k_1\right)}}, b_1 = 0, B = \delta^{\frac{1}{\sqrt{2}}},$$
$$j_1 = \frac{d_1\left(3\nu\log^2(\delta) - 2\nu^3\right) - 2\left(AP + \lambda + \nu s_1 - \epsilon^2\right)}{2\nu^2 - \log^2(\delta)}. \tag{3.10}$$

By putting set 2 in Eq (3.5), we obtain the exact solution as follows:

$$\mathfrak{Q}_4(\xi) = \frac{\sqrt{2}\,\sqrt{\eta}\log(\delta)\sqrt{AP - 2d_1\nu^3 + \lambda + \nu s_1 - \epsilon^2}}{\left(H\log\left(\delta^{\frac{1}{\sqrt{2}}}\right)\delta^{\frac{x - t\omega_0}{\sqrt{2}}} + \frac{\eta\delta^{-\frac{x - t\omega_0}{\sqrt{2}}}}{4H\log\left(\delta^{\frac{1}{\sqrt{2}}}\right)}\right)\sqrt{\left(\log^2(\delta) - 2\nu^2\right)\left(\nu\left(m_1 - \alpha_1 A^2\left(l_1 + \nu n_1\right)\right) + k_1\right)}}. \tag{3.11}$$

When we choose B = e and $\eta = 4H^2$, the Eq (3.11) is

$$\mathfrak{Q}_5(\xi) = \frac{4\sqrt{H^2}\log^2(\delta)\delta^{\frac{t\omega_0 + x}{\sqrt{2}}}\sqrt{AP - 2d_1\nu^3 + \lambda + \nu s_1 - \epsilon^2}}{H\left(2\delta^{\sqrt{2}t\omega_0} + \log^2(\delta)\delta^{\sqrt{2}x}\right)\sqrt{\left(\log^2(\delta) - 2\nu^2\right)\left(\nu\left(m_1 - \alpha_1 A^2\left(l_1 + \nu n_1\right)\right) + k_1\right)}}. \tag{3.12}$$

When we choose B = e and $\eta = -4H^2$, the Eq (3.11) is

$$\mathfrak{Q}_6(\xi) = -\frac{4H\log^2(\delta)\delta^{\frac{t\omega_0 + x}{\sqrt{2}}}\sqrt{AP - 2d_1\nu^3 + \lambda + \nu s_1 - \epsilon^2}}{\sqrt{-H^2}\left(\log^2(\delta)\delta^{\sqrt{2}x} - 2\delta^{\sqrt{2}t\omega_0}\right)\sqrt{\left(\log^2(\delta) - 2\nu^2\right)\left(\nu\left(m_1 - \alpha_1 A^2\left(l_1 + \nu n_1\right)\right) + k_1\right)}}. \tag{3.13}$$

Set 03.

$$a_0 = 0, a_1 = \frac{\sqrt{2}\,\sqrt{\eta}\log(\delta)\sqrt{AP - 2d_1\nu^3 + \lambda + \nu s_1 - \epsilon^2}}{\sqrt{\left(\log^2(\delta) - 2\nu^2\right)\left(\nu\left(m_1 - \alpha_1 A^2\left(l_1 + \nu n_1\right)\right) + k_1\right)}}, b_1 = 0, B = \delta^{-\frac{1}{\sqrt{2}}},$$
$$j_1 = \frac{d_1\left(3\nu\log^2(\delta) - 2\nu^3\right) - 2\left(AP + \lambda + \nu s_1 - \epsilon^2\right)}{2\nu^2 - \log^2(\delta)}. \tag{3.14}$$

By putting set 3 in Eq (3.5), we obtain the exact solution as follows:

$$\mathfrak{Q}_7(\xi) = \frac{\sqrt{2}\,\sqrt{\eta}\log(\delta)\sqrt{AP - 2d_1\nu^3 + \lambda + \nu s_1 - \epsilon^2}}{\left(H\log\left(\delta^{-\frac{1}{\sqrt{2}}}\right)\delta^{-\frac{x - t\omega_0}{\sqrt{2}}} + \frac{\eta\delta^{\frac{x - t\omega_0}{\sqrt{2}}}}{4H\log\left(\delta^{-\frac{1}{\sqrt{2}}}\right)}\right)\sqrt{\left(\log^2(\delta) - 2\nu^2\right)\left(\nu\left(m_1 - \alpha_1 A^2\left(l_1 + \nu n_1\right)\right) + k_1\right)}}. \tag{3.15}$$

When we choose B = e and $\eta = 4H^2$, the Eq (3.15) is

$$\mathfrak{Q}_8(\xi) = -\frac{4\sqrt{H^2}\log^2(\delta)\delta^{\frac{t\omega_0 + x}{\sqrt{2}}}\sqrt{AP - 2d_1\nu^3 + \lambda + \nu s_1 - \epsilon^2}}{H\left(\log^2(\delta)\delta^{\sqrt{2}t\omega_0} + 2\delta^{\sqrt{2}x}\right)\sqrt{\left(\log^2(\delta) - 2\nu^2\right)\left(\nu\left(m_1 - \alpha_1 A^2\left(l_1 + \nu n_1\right)\right) + k_1\right)}}. \tag{3.16}$$

When we choose F = e and $\epsilon = -4\beta^2$, the Eq (3.15) is

$$\mathfrak{Q}_9(\xi) = \frac{4H\log^2(\delta)\delta^{\frac{t\omega_0+x}{\sqrt{2}}}\sqrt{AP - 2d_1\nu^3 + \lambda + \nu s_1 - \epsilon^2}}{\sqrt{-H^2}\left(\log^2(\delta)\delta^{\sqrt{2}t\omega_0} - 2\delta^{\sqrt{2}x}\right)\sqrt{\left(\log^2(\delta) - 2\nu^2\right)\left(\nu\left(m_1 - \alpha_1 A^2\left(l_1 + \nu n_1\right)\right) + k_1\right)}}. \tag{3.17}$$

The analytical solutions derived through the generalized Arnous method are illustrated in Figures 1–3, which depict distinct soliton structures, including kink, bright, and rational waves. These graphical representations validate the obtained results and provide visual insight into the nonlinear wave behavior discussed in the following sections.

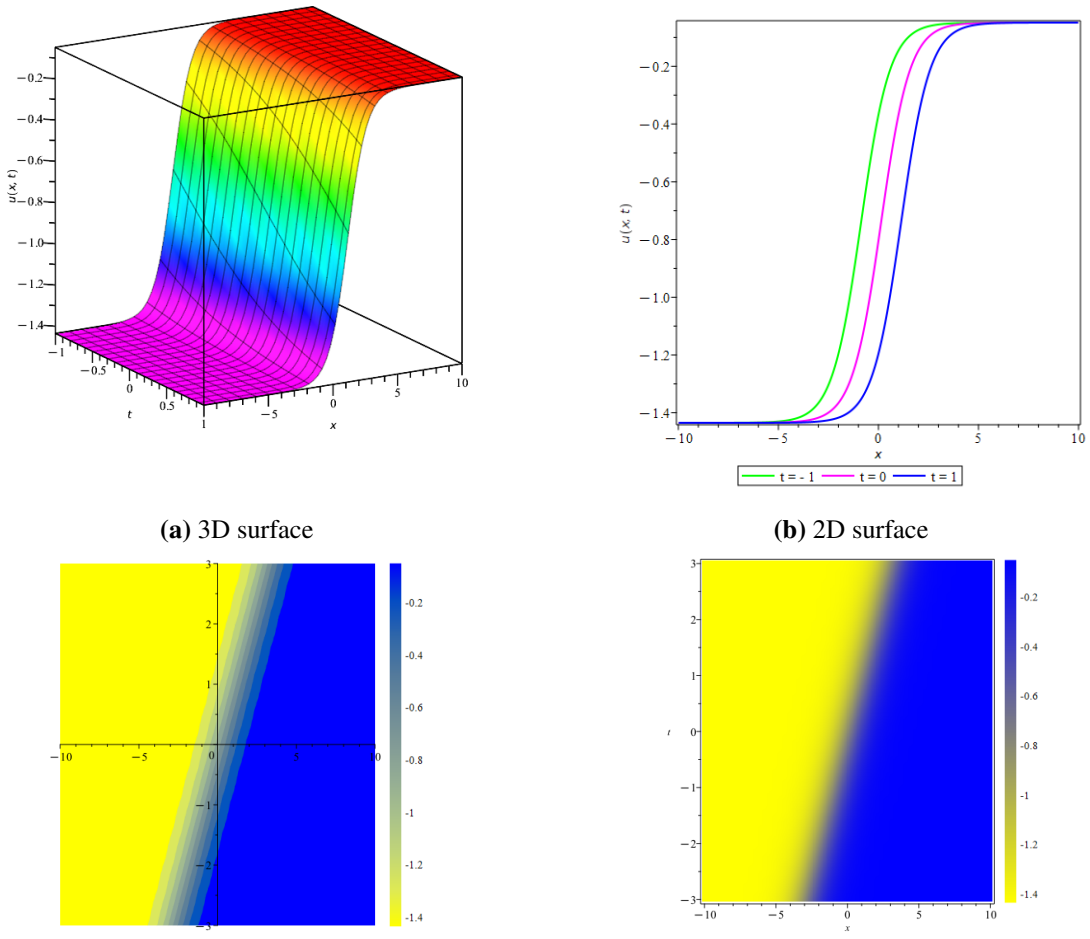

(a) 3D surface **(b)** 2D surface

(c) Contour plot **(d)** Density plot

Figure 1. Graphical visualization of the derived solution of Eq (3.7), including (a) 3D surface plot, (b) 2D surface plot, (c) contour plot, and (d) density plot of $\mathfrak{Q}_{01}(t, x)$ with parameters $B = 0.5$, $b_1 = 1$, $\omega_0 = 1$, $H = 0.1$, $\eta = 2$, $\delta = 2$, $\nu = -1$, $n_1 = 1$, $k_1 = 0.3$, $d_1 = 2$, $A = 1$, $P = 1$, $s_1 = -1$, $l_1 = 2$, $\epsilon = 0.5$, $m_1 = 0.1$, $\alpha_1 = 2$, and $\lambda = 0.5$.

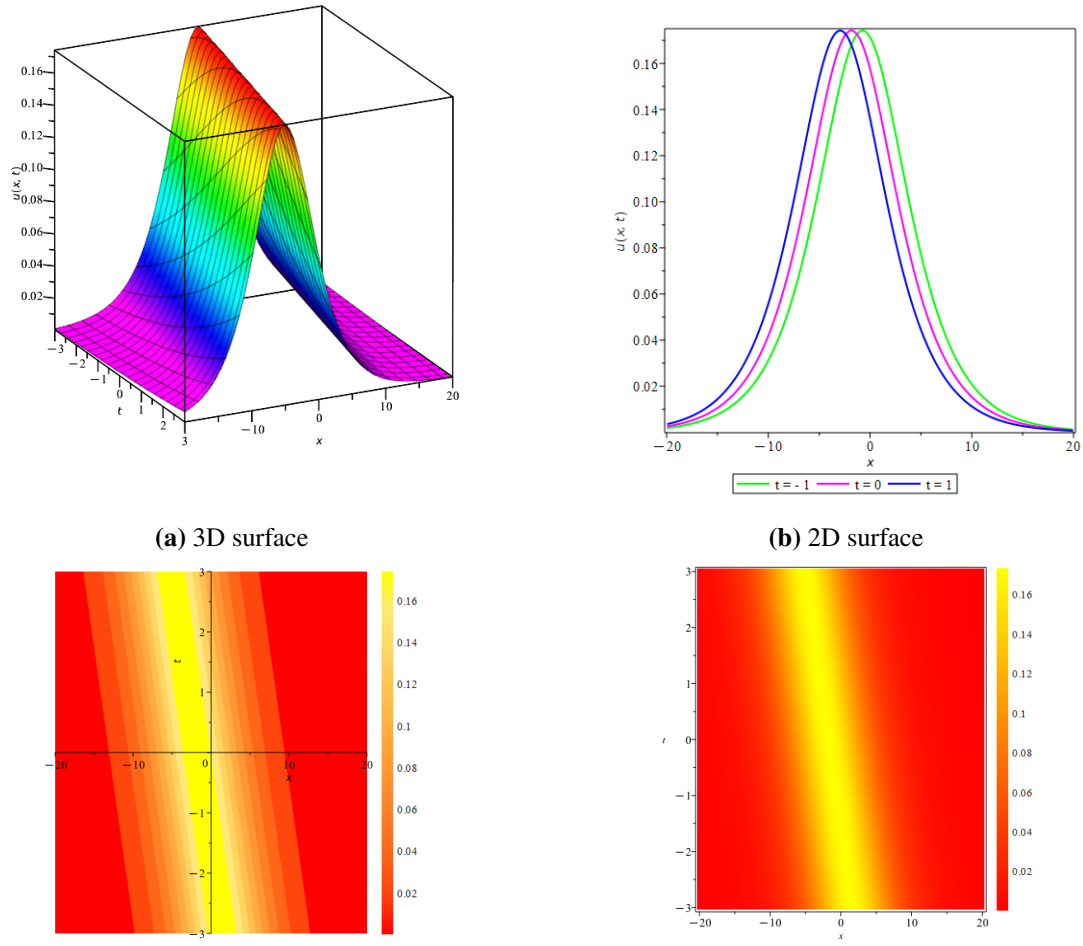

(a) 3D surface **(b)** 2D surface

(c) Contour plot **(d)** Density plot

Figure 2. Graphical visualization of the derived solution of Eq (3.11), including (a) 3D surface plot, (b) 2D surface plot, (c) contour plot, and (d) density plot of $Q_{07}(t, y, x)$ with parameters $B = -1$, $b_1 = 1.1$, $\omega_0 = -1.1$, $H = 1$, $\eta = 0.4$, $\delta = 1.5$, $\nu = 1$, $n_1 = 0.01$, $k_1 = 0.3$, $d_1 = 0.3$, $A = 0.3$, $P = 1.5$, $s_1 = 1$, $l_1 = 2$, $\epsilon = 1.5$, $m_1 = 1.1$, $\alpha_1 = 1$, and $\lambda = 0.1$.

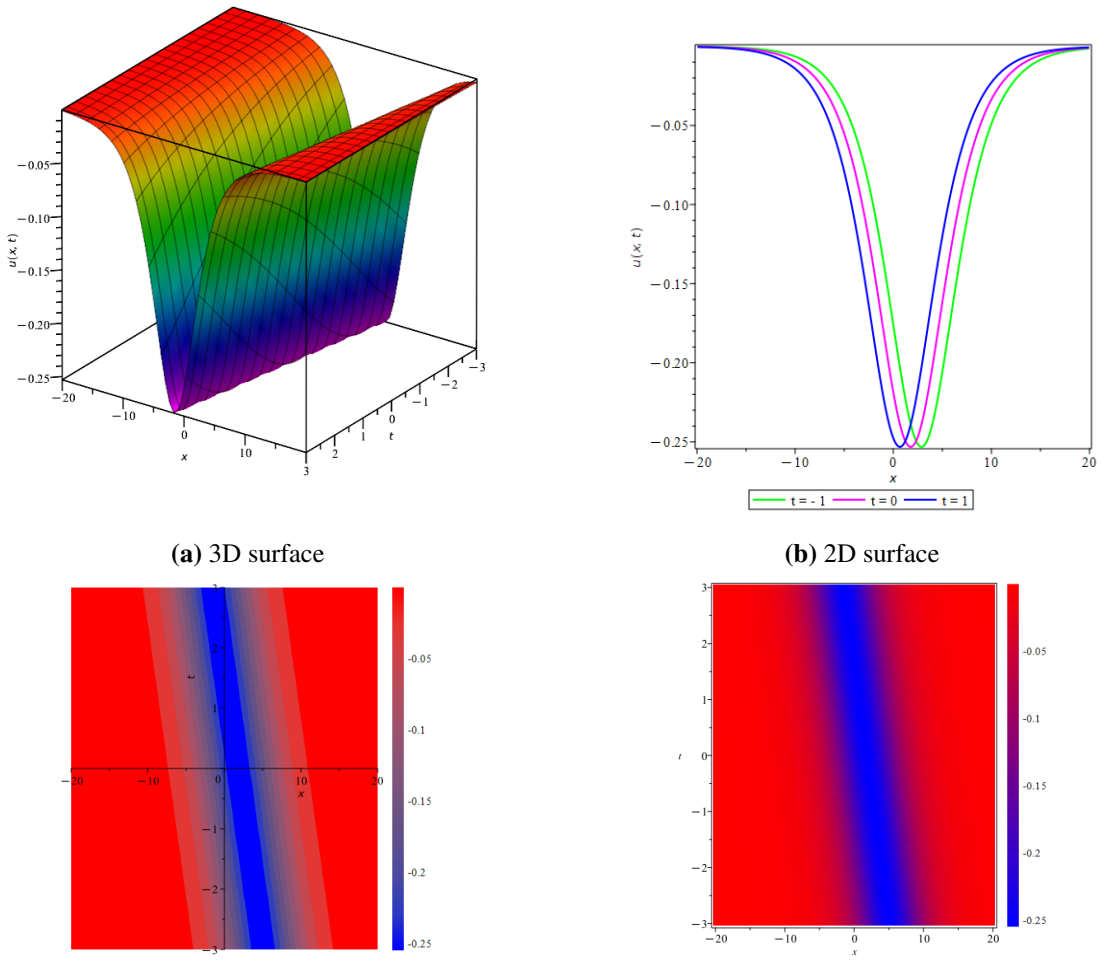

(a) 3D surface **(b)** 2D surface

(c) Contour plot **(d)** Density plot

Figure 3. Graphical visualization of the derived solution of Eq (3.15), including (a) 3D surface plot, (b) 2D surface plot, (c) contour plot, and (d) density plot of $Q_{10}(t, y, x)$ with parameters $B = -1$, $b_1 = 1.1$, $\omega_0 = -1.1$, $H = 1$, $\eta = 0.4$, $\delta = 0.6$, $\nu = 1$, $n_1 = 0.01$, $k_1 = 0.3$, $d_1 = 0.3$, $A = 0.3$, $P = 1.5$, $s_1 = 1$, $l_1 = 2$, $\epsilon = 1.5$, $m_1 = 1.1$, $\alpha_1 = 1$, and $\lambda = 0.1$.

3.2. Advantages of the GA method

The GA method offers several methodological advantages. It gives exact analytical solutions, such as trigonometric, exponential, and soliton forms, that explain system behavior more directly than numerical results. The procedure remains relatively straightforward, as the balancing step and subsequent algebraic manipulations are less demanding, unlike other, more complicated methods. Furthermore, the GA method is versatile, capable of generating diverse families of solitary wave solutions within a unified framework. Having explicit solutions also makes it easier to study stability and bifurcations, offering insights that numerical work alone cannot provide.

3.3. Limitations of the GA method

Although the GA method is powerful, it cannot be applied to all classes of nonlinear PDEs. Its effectiveness depends on the ability to balance the high-order derivative with nonlinear terms. When this balance cannot be established, the method may fail to yield meaningful solutions. Such limitations commonly occur in equations with irregular structures, pronounced nonlocal effects, or discontinuities. In particular, models involving fractional derivatives, stochastic elements, or piecewise-defined nonlinearities often lie outside the scope of the GA framework. In such cases, alternative methods such as homotopy analysis, variational iteration, or numerical schemes may be more suitable.

4. Dynamical analysis of the governing equation

4.1. Phase portraits analysis

This subsection focuses on the phase plane analysis of the generalized stochastic Schrödinger–Hirota equation. Phase portrait analysis [55] is a powerful qualitative technique for dynamical systems. By applying the Galilean transformation, the system $\mathcal{R}'_1 = \mathcal{G}$ on Eq (2.16). The following system of differential equations is equivalent to Eq (2.16):

$$\begin{cases} \dfrac{d\mathcal{R}_1}{d\xi} = \mathcal{G}, \quad \dfrac{d\mathcal{G}}{d\xi} = -\mathfrak{B}_1\mathcal{R}_1^3 + \mathfrak{B}_2\mathcal{R}_1, \\ \mathfrak{B}_1 = \dfrac{k_1 + m_1\nu - \alpha_1\nu(l_1 + n_1\nu)A^2}{j_1 + 3d_1\nu}, \quad \mathfrak{B}_2 = \dfrac{\lambda - \epsilon^2 + j_1\nu^2 + d_1\nu^3 + s_1\nu + AP}{j_1 + 3d_1\nu}. \end{cases} \tag{4.1}$$

To find the equilibrium points of the system (4.1), we solve as follows:

$$\begin{cases} \mathcal{G} = 0, \\ -\mathfrak{B}_1\mathcal{R}_1^3 + \mathfrak{B}_2\mathcal{R}_1 = 0. \end{cases} \tag{4.2}$$

As a consequence, we obtain three equilibrium points as follows:

$$\mathcal{A}_0 = (\mathcal{S}_0, 0)\,,\ \mathcal{A}_1 = (\mathcal{S}_1, 0)\,,\ \mathcal{A}_2 = (\mathcal{S}_2, 0)\,,$$

where $\mathcal{S}_0 = 0$, $\mathcal{S}_1 = \sqrt{\frac{\mathfrak{B}_2}{\mathfrak{B}_1}}$, and $\mathcal{S}_2 = -\sqrt{\frac{\mathfrak{B}_2}{\mathfrak{B}_1}}$. Jacobian matrix of the system (4.1) can be written as:

$$\mathcal{J}(\mathcal{R}_1, \mathcal{G}) = \begin{vmatrix} 0 & 1 \\ -3\mathfrak{B}_1\mathcal{R}_1^2 + \mathfrak{B}_2 & 0 \end{vmatrix} = (3\mathfrak{B}_1\mathcal{R}_1^2 - \mathfrak{B}_2)\cdot$$

Proposition 1: As a consequence, point $(\mathbf{S}_0, 0)$ represents the saddle point if $\mathcal{J}(\mathcal{A}_0)$ is less than zero, indicates a center behavior if $\mathcal{J}(\mathcal{A}_0)$ is greater than zero, and $(\mathbf{S}_0, 0)$ shows a cusp behavior if $\mathcal{J}(\mathcal{A}_0)$ is equally to zero. Similarly, point $(\mathbf{S}_1, 0)$ represents the saddle point if $\mathcal{J}(\mathcal{A}_1)$ is less than zero, indicates a center behavior if $\mathcal{J}(\mathcal{A}_1)$ is greater than zero, and $(\mathbf{S}_1, 0)$ shows a cusp behavior if $\mathcal{J}(\mathcal{A}_1)$ is equal to zero. Likewise, the third point has the same condition.

Family 1: When $\mathfrak{B}_1 < 0$, $\mathfrak{B}_2 > 0$.

Equation (4.1) has three equilibrium points. For $(\mathcal{S}_0, 0)$, $\mathcal{J}(A_0) = -\mathfrak{B}_2$, since, in this case, $\mathfrak{B}_2$ is positive. So, $\mathcal{J}(A_0) < 0$; therefore, $(\mathcal{S}_0, 0)$ is a saddle point. For $(\mathcal{S}_1, 0)$, $\mathcal{J}(A_1) = 2\mathfrak{B}_2$, since, in this case, $\mathfrak{B}_2$ is positive. So, $\mathcal{J}(A_0) > 0$; therefore, $(\mathcal{S}_1, 0)$ is a center point. Similarly, $(\mathcal{S}_2, 0)$ is also a center point, which is shown in Figure 4.

Family 2: When $\mathfrak{B}_1 < 0$, $\mathfrak{B}_2 < 0$.

Equation (4.1) has three equilibrium points. For $(\mathcal{S}_0, 0)$, $\mathcal{J}(A_0) = \mathfrak{B}_2$, since, in this case, $\mathfrak{B}_2$ is negative. So, $\mathcal{J}(A)_0 > 0$; therefore, $(\mathcal{S}_0, 0)$ is a center point. For $(\mathcal{S}_1, 0)$, $\mathcal{J}(A_1) = 2\mathfrak{B}_2$, since, in this case, $\mathfrak{B}_2$ is negative. So, $\mathcal{J}(A_0) < 0$; therefore, $(\mathcal{S}_1, 0)$ is a saddle point. Similarly, $(\mathcal{S}_2, 0)$ is also a saddle point, which is demonstrated in Figure 4.

Equation (4.1) has three equilibrium points. For $(\mathcal{S}_0, 0)$, $\mathcal{J}(A_0) = -\mathfrak{B}_2$, since, in this case, $\mathfrak{B}_2$ is negative. So, $\mathcal{J}(A)_0 > 0$; therefore, $(\mathcal{S}_0, 0)$ is a center point. For $(\mathcal{S}_1, 0)$, $\mathcal{J}(A_1) = 2\mathfrak{B}_2$, since, in this case, $\mathfrak{B}_2$ is negative. So, $\mathcal{J}(A_0) < 0$; therefore, $(\mathcal{S}_1, 0)$ is a saddle point. Similarly $(\mathcal{S}_2, 0)$, is also a saddle point.

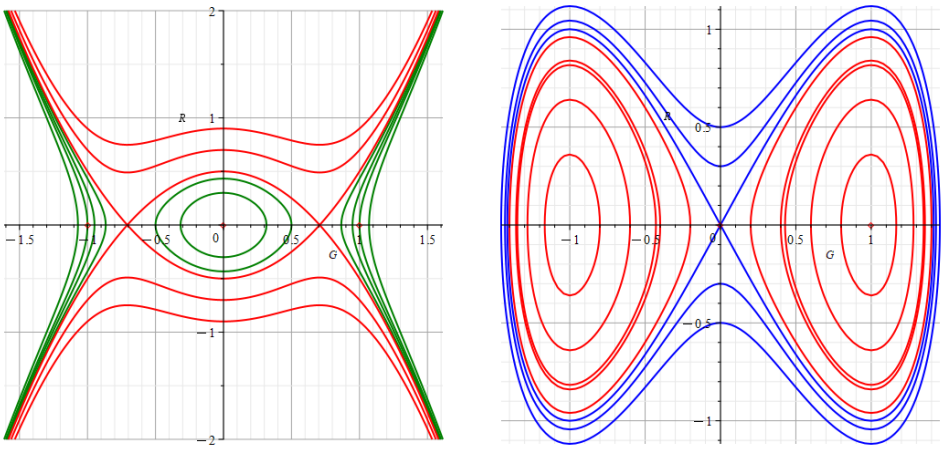

(a) $\mathfrak{B}_1 < 0$, $\mathfrak{B}_2 < 0$ **(b)** $\mathfrak{B}_1 < 0$, $\mathfrak{B}_2 > 0$

Figure 4. Phase trajectory analysis in two-dimensional plots for the unperturbed system (4.1).

4.2. Chaotic dynamics

In the present investigation, we employed the chaotic dynamics exhibited by the planar dynamical system delineated in Eq (4.1) through the incorporation of the perturbation term $\mathcal{T}\cos(\mathcal{K}\xi)$. The system represented by Eq (4.1) can be expressed as [56, 57]:

$$\begin{cases} \dfrac{d\mathcal{R}_1}{d\xi} = \mathcal{G}, & \dfrac{d\mathcal{G}}{d\xi} = -\mathfrak{B}_1\mathcal{R}_1^3 + \mathfrak{B}_2\mathcal{R}_1 + \mathcal{T}\cos(\mathcal{K}\xi). \end{cases} \tag{4.3}$$

where $\mathfrak{B}_2 = \frac{\lambda - \epsilon^2 + j_1\nu^2 + d_1\nu^3 + s_1\nu + AP}{j_1 + 3d_1\nu}$ and $\mathfrak{B}_1 = \frac{k_1 + m_1\nu - \alpha_1\nu(l_1 + n_1\nu)A^2}{j_1 + 3d_1\nu}$. Consequently, $\mathcal{T}$ represents the frequency, while $\mathcal{K}$ denotes the amplitude of the external force that exerts influence on the dynamic system delineated in Eq (4.1). We present the 2D phase portraits, 3D phase portraits, time series, and Poincaré map. In Figure 5, it is evident that the system described by Eq (4.3) is quasi-periodic, as part (c) of Figure 5 depicts a closed curve, based on the chosen parametric values $\mathcal{B}_1 = 0.5$, $\mathcal{B}_2 = 3.3$, $\mathcal{T} = 0.2$,

and $\mathcal{K} = 0.08$ and the initial conditions $(R_1, G) = (2.67, 1.1)$. In Figure 6, it is shown that system Eq (4.3) is quasi-periodic, as part (c) of Figure 6 also depicts a closed curve, based on varying the initial conditions $(R_1, G) = (1.09, 0.01)$. Similarly, Figure 7 also depicts chaotic behavior, since part (c) of Figure 7 exhibits a torus when using the parametric values $\mathcal{B}_1 = 2.5$, $\mathcal{B}_2 = 3.3$, $\mathcal{T} = 0.09$, and $\mathcal{K} = 0.06$ and the initial conditions $(R_1, G) = (1.9, 0.01)$.

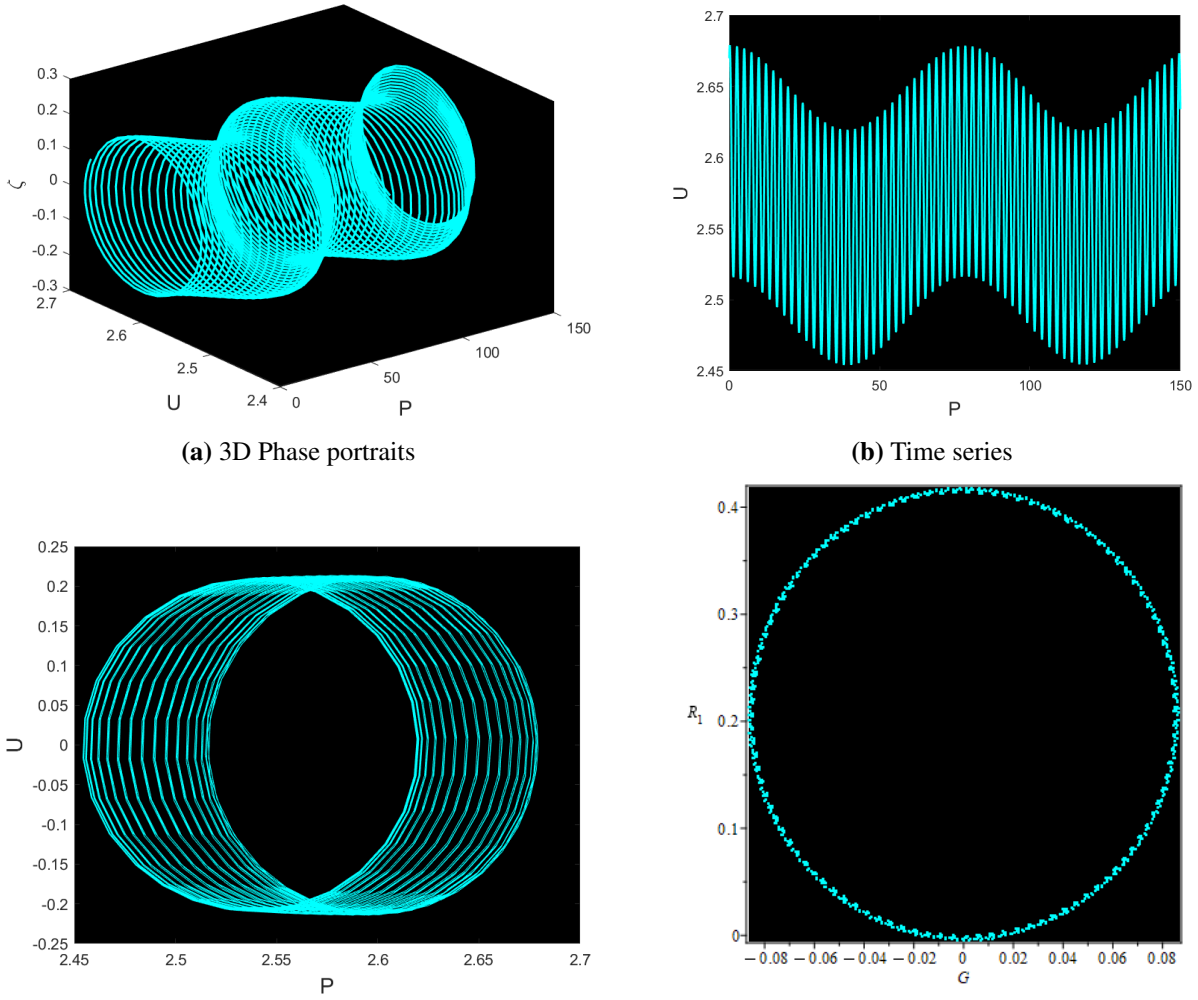

(a) 3D Phase portraits

(b) Time series

(c) 2D Phase portraits

(d) Poincare map

Figure 5. Chaotic behavior of system (4.3) using parameters $\mathcal{B}_1 = 0.5$, $\mathcal{B}_2 = 3.3$, $\mathcal{T} = 0.2$, and $\mathcal{K} = 0.08$ and initial conditions $(R_1, G) = (2.67, 1.1)$.

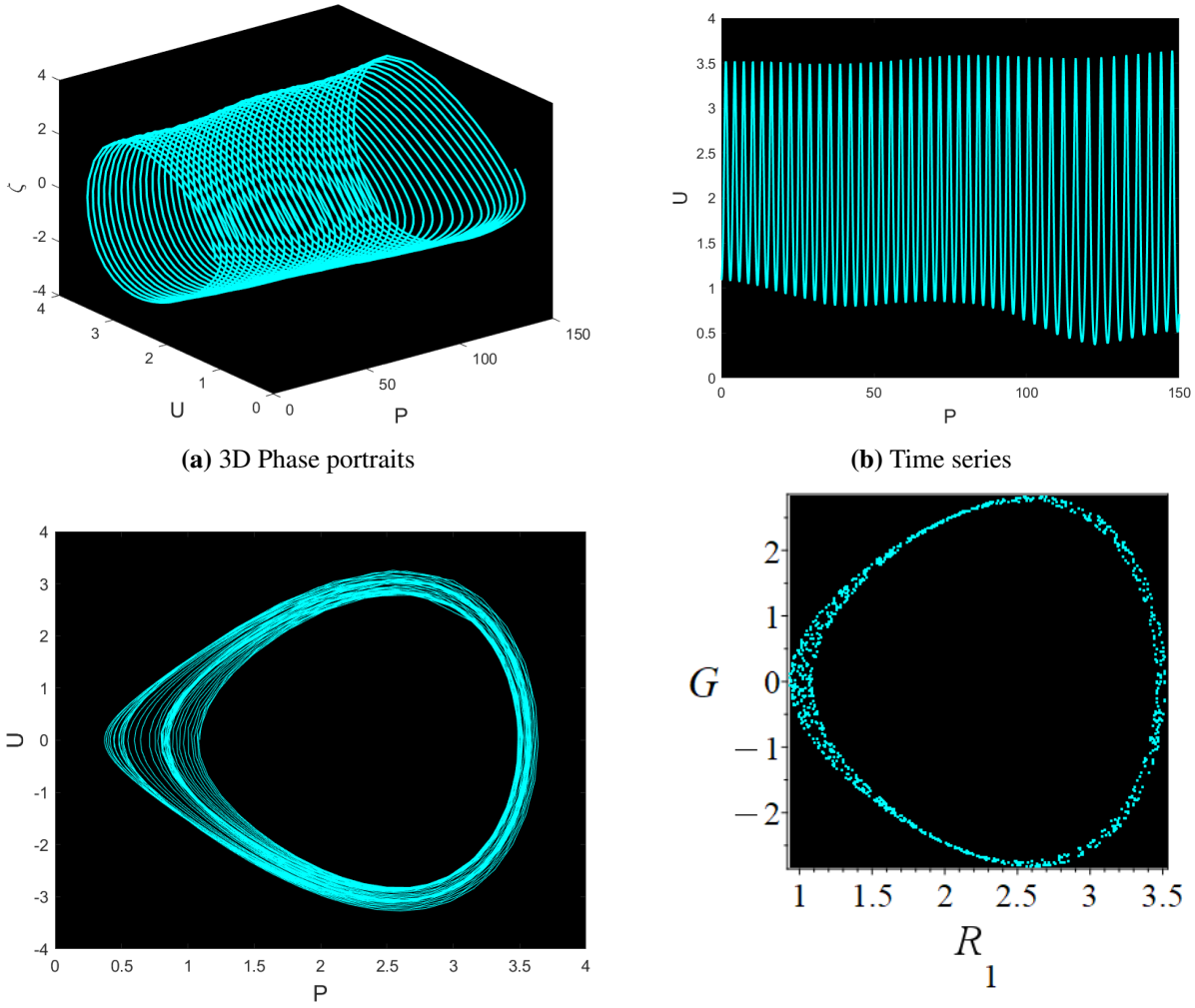

(a) 3D Phase portraits

(b) Time series

(c) 2D Phase portraits

(d) Poincare map

Figure 6. Chaotic behavior of system (4.3) using parameters $\mathcal{B}_1 = 0.5$, $\mathcal{B}_2 = 3.3$, $\mathcal{T} = 0.2$, and $\mathcal{K} = 0.08$ and initial conditions $(R_1, G) = (1.09, 0.01)$.

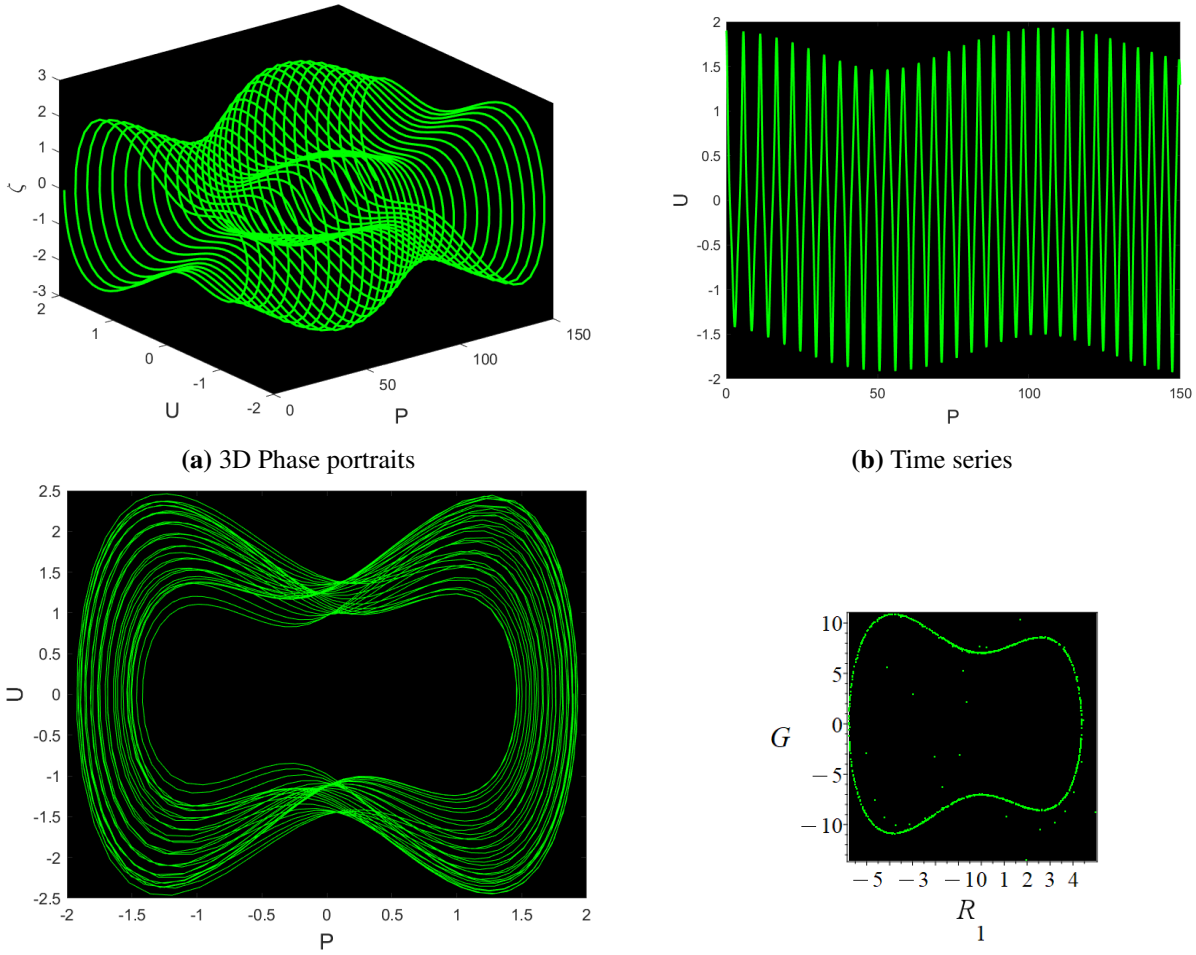

(a) 3D Phase portraits

(b) Time series

(c) 2D Phase portraits

(d) Poincare map

Figure 7. Chaotic behavior of system (4.3) using parameters $\mathcal{B}_1 = 2.5$, $\mathcal{B}_2 = 3.3$, $\mathcal{T} = 0.09$, and $\mathcal{K} = 0.06$ and initial conditions $(R_1, G) = (1.9, 0.01)$.

4.3. Multistability analysis

In this section, we will evaluate the multistability analysis of system Eq (4.3). Multistability analysis refers to the presence of two or more coexisting outcomes, representing the system's flexibility under a constrained set of parameter options and varying the initial conditions [58,59]. Our analysis will focus on the specific nature of multistability in the system Eq (4.3), utilizing phase portraits to gain deeper insight into its dynamics. In Figure 8(a), we present two separate images for the parameters $\mathcal{B}_1 = 0.5$, $\mathcal{B}_2 = 3.3$, $\mathcal{T} = 0.2$, and $\mathcal{K} = 0.08$, where the initial conditions $(R_1, G) = (2.67, 0.1)$ are represented in red and the initial conditions $(R_1, G) = (2.57, 0.1)$ are represented in blue. In Figure 8(b), we present two separate images for the parameters $\mathcal{B}_1 = 2.5$, $\mathcal{B}_2 = 3.3$, $\mathcal{T} = 0.9$, and $\mathcal{K} = 0.06$, where the initial conditions $(R_1, G) = (1.95, 0.01)$ are represented in red and initial conditions $(R_1, G) = (1.9, 0.1)$ are represented in blue.

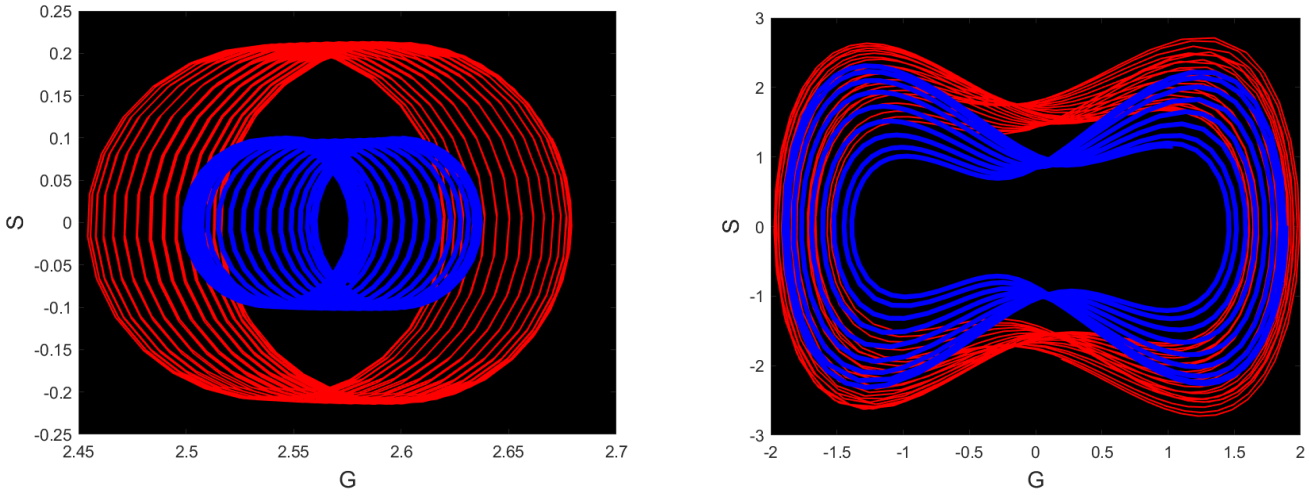

(a) 2D phase portraits; initial conditions $(R_1, G) = (2.67, 0.1)$ in red and $(R_1, G) = (2.57, 0.1)$ in blue.

(b) 2D phase portraits; initial conditions $(R_1, G) = (1.95, 0.01)$ in red and $(R_1, G) = (1.9, 0.1)$ in blue.

Figure 8. Multistability of system Eq (4.3) showing different 2D phase portraits corresponding to different initial conditions.

4.4. Lyapunov exponents

Lyapunov exponents quantitatively assess the exponential divergence or convergence of proximate trajectories within a dynamical system, thereby elucidating the system's stability and predictability. A positive Lyapunov exponent indicates chaotic dynamics with sensitivity to initial conditions. In contrast, negative exponents would indicate stability. Basically, these exponents are the prime discriminators for chaos and regular behavior, and they give a measure of unpredictability linked to the dynamic systems in question. The use of these exponents spans a broad horizon of fields, such as physics, engineering, biology, finance, etc. They are the tools for stability analyses in control systems and for complex behavior patterns in climate modeling and neuroscience. Besides, Lyapunov exponents are employed in the study of chaotic time series and for phenomena related to turbulence in fluid dynamics. Figures 9 and 10 demonstrate chaos in system (4.3) using Lyapunov exponents with $\mathfrak{B}_1 = 0.6, \mathfrak{B}_2 = -0.6, \mathcal{T} = 0.5, \mathcal{K} = 0.96$, and varying initial conditions.

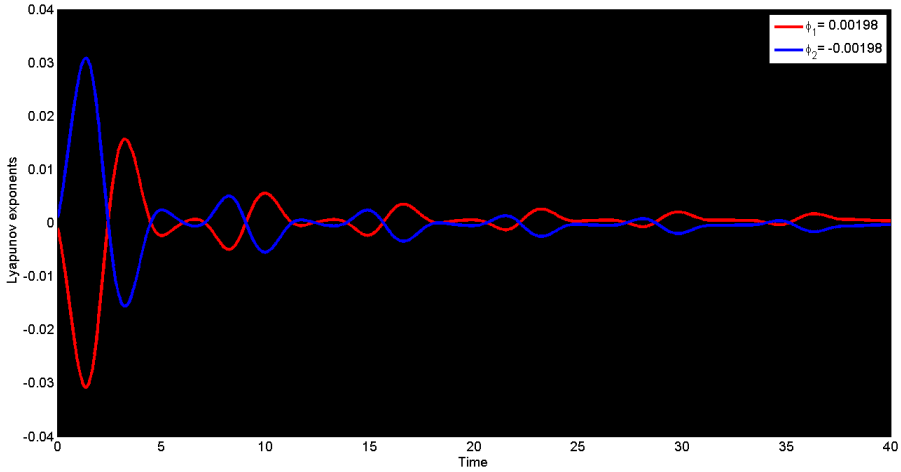

Figure 9. Examining chaos in system (4.3) using Lyapunov exponents with parameters $\mathfrak{B}_1 = 0.6$, $\mathfrak{B}_2 = -0.6$, $\mathcal{T} = 0.5$, $\mathcal{K} = 0.96$, and initial conditions $(0.03, 0.03, 0.03)$.

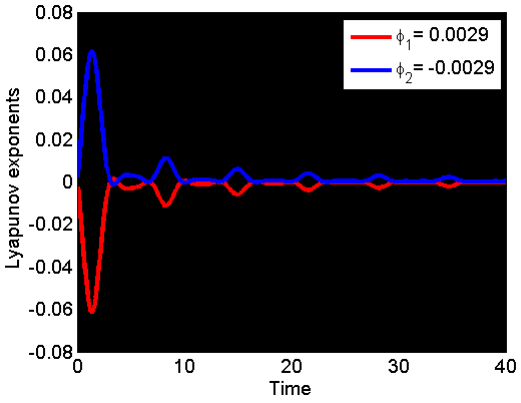

Figure 10. Examining chaos in system (4.3) using Lyapunov exponents with parameters $\mathfrak{B}_1 = 0.6$, $\mathfrak{B}_2 = -0.6$, $\mathcal{T} = 0.5$, $\mathcal{K} = 0.96$, and initial conditions $(0.03, 0.03, 0.03)$.

4.5. Sensitivity demonstration

To evaluate the model's sensitivity, this section examines how the proposed equation responds to variations in initial conditions.

$$\begin{cases} \dfrac{d\mathcal{R}_1}{d\xi} = \mathcal{G}, \quad \dfrac{d\mathcal{G}}{d\xi} = -\mathfrak{B}_1\mathcal{R}_1^3 + \mathfrak{B}_2\mathcal{R}_1. \end{cases} \tag{4.4}$$

In this phase of the study, we conduct a detailed sensitivity analysis of the dynamical system described by Eq (4.4), considering two distinct sets of initial conditions. The resulting solutions are illustrated in figures using relevant parameter values, including $\mathcal{B}_1 = 0.6$ and $\mathcal{B}_2 = 1.3$. Figures 11 and 12 illustrate the analysis of two sets of initial conditions, while Figure 13 explores three additional sets. Figures 11 depicts two solutions by utilizing the various initial conditions $(\mathcal{G}, \mathcal{R}_1) = (0.5, 5.02)$ in green and $(\mathcal{G}, \mathcal{R}_1) = (1.02, 8.02)$ in red. Figure 12 depicts two solutions by utilizing the various initial conditions

$(\mathcal{G}, \mathcal{R}_1) = (0.5, 5.02)$ in green and $(\mathcal{G}, \mathcal{R}_1) = (7.02, 2.2)$ in magenta. Figure 13 shows three two solutions by utilizing the various initial conditions $(\mathcal{G}, \mathcal{R}_1) = (0.5, 5.02)$ in green $(\mathcal{G}, \mathcal{R}_1) = (7.02, 2.2)$ in magenta, and $(\mathcal{G}, \mathcal{R}_1) = (1.02, 8.02)$ in red. These results reveal that even small adjustments in initial conditions can lead to subtle changes in the system's dynamics. The solution curves notably do not overlap, indicating that the proposed system exhibits a degree of sensitivity. Understanding this sensitivity is crucial, as it highlights the impact of initial conditions on outcomes, thereby enhancing the model's predictive accuracy and robustness across diverse applications. The initial conditions for sensitivity analysis were chosen as small perturbations of the soliton profile. This choice reflects the practical situation in optical communication systems, where unavoidable fluctuations in the initial pulse shape and amplitude are present. By selecting nearby initial states, we can demonstrate how such small deviations evolve under the system dynamics. In particular, the positive Lyapunov exponents show that these perturbations grow over time, confirming the sensitivity to initial conditions and the presence of chaotic dynamics.

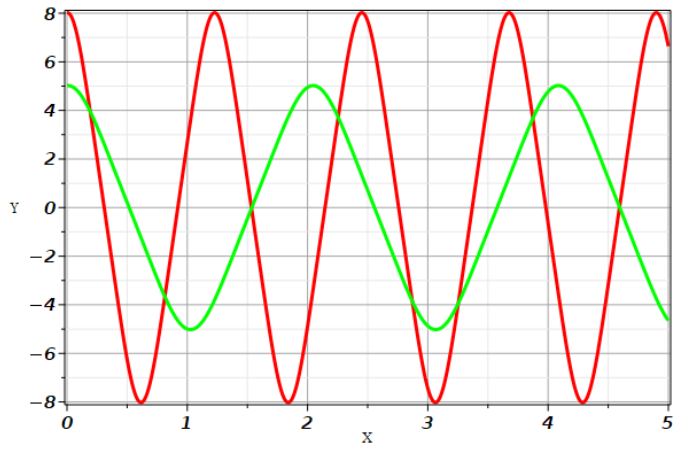

Figure 11. Sensitivity analysis of Eq (4.4) using different initial conditions: $(\mathcal{G}, \mathcal{R}_1) = (0.5, 5.02)$ in green and $(\mathcal{G}, \mathcal{R}_1) = (1.02, 8.02)$ in red.

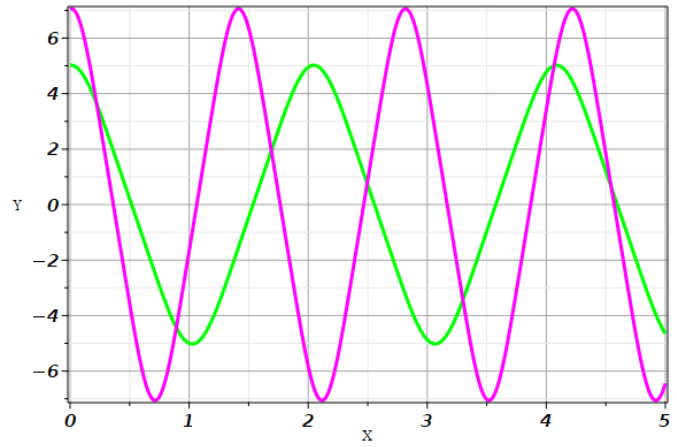

Figure 12. Sensitivity analysis of Eq (4.4) using different initial conditions: $(\mathcal{G}, \mathcal{R}_1) = (0.5, 5.02)$ in green and $(\mathcal{G}, \mathcal{R}_1) = (7.02, 2.2)$ in magenta.

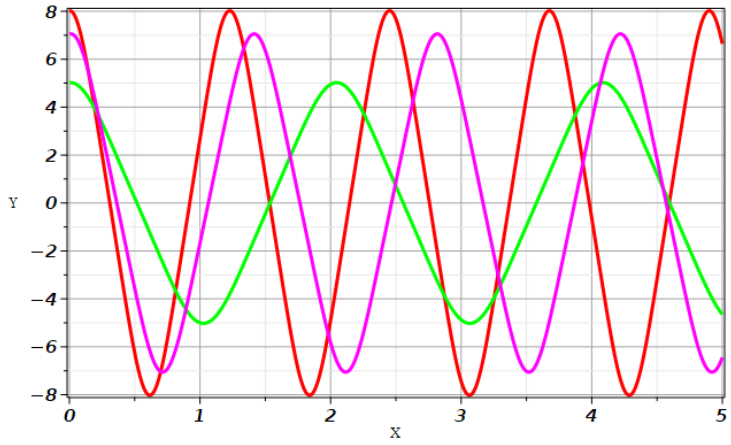

Figure 13. Sensitivity analysis of Eq (4.4) using different initial conditions: $(\mathcal{G}, \mathcal{R}_1) = (0.5, 5.02)$ in green, $(\mathcal{G}, \mathcal{R}_1) = (7.02, 2.2)$ in magenta, and $(\mathcal{G}, \mathcal{R}_1) = (1.02, 8.02)$ in red.

5. Results and discussion

The graphical results are presented in Figures 1–3, which correspond to the different physical soliton structures, each carrying specific meanings in nonlinear wave dynamics. Figure 1, with the parameters $B = 0.5$, $b_1 = 1$, $\omega_0 = 1$, $H = 0.1$, $\eta = 2$, $\delta = 2$, $\nu = -1$, $n_1 = 1$, $k_1 = 0.3$, $d_1 = 2$, $A = 1$, $P = 1$, $s_1 = -1$, $l_1 = 2$, $\epsilon = 0.5$, $m_1 = 0.1$, $\alpha_1 = 2$, and $\lambda = 0.5$, represents kink-type solution. Kink solitons link two asymptotic states in a step-like profile, representing domain walls or transition layers in nonlinear materials. A higher dispersion coefficient d_1 broadens the Kink's transition region, while the coupling parameters (e.g., k_1, m_1) make the front steeper. An increase in the velocity (ω_0) leads to the faster translational motion while preserving the overall kink profile in the coordinates x and t. The noise intensity ϵ acts as an effective damping factor: for moderate levels (e.g., ϵ= 0.5), the kink remains visible but with a slightly weaker gradient as $\epsilon \approx 0$; at high values, the step becomes blurred.

Figure 2, with parameters $B = -1$, $b_1 = 1.1$, $\omega_0 = -1.1$, $H = 1$, $\eta = 0.4$, $\delta = 1.5$, $\nu = 1$, $n_1 = 0.01$, $k_1 = 0.3$, $d_1 = 0.3$, $A = 0.3$, $P = 1.5$, $s_1 = 1$, $l_1 = 2$, $\epsilon = 1.5$, $m_1 = 1.1$, $\alpha_1 = 1$, and $\lambda = 0.1$, represents tanh-type bright soliton. These solutions exhibit maximum amplitude at the center and approach a constant value background at infinity, which makes them well-suited for describing optical pulse transmission in nonlinear optical fibers. The pulse amplitude depends on the factor b_1 and the nonlinear coefficients (k_1, m_1); a larger value leads to higher and narrower peaks. Increasing dispersion d_1 makes the pulse wider and lowers its peak, reflecting the dispersion nonlinearity balance. Noise intensity ϵ affects amplitude decay: at moderate noise (e.g., $\epsilon = 0.5$), the envelope decays more slowly than in the noiseless case (ϵ =0), helping the pulse to stay stable for a while. At large noise amplitudes, fluctuations increase and coherence degrades.

Figure 3 with parameters $B = -1$, $b_1 = 1.1$, $\omega_0 = -1.1$, $H = 1$, $\eta = 0.4$, $\delta = 0.6$, $\nu = 1$, $n_1 = 0.01$, $k_1 = 0.3$, $d_1 = 0.3$, $A = 0.3$, $P = 1.5$, $s_1 = 1$, $l_1 = 2$, $\epsilon = 1.5$, $m_1 = 1.1$, $\alpha_1 = 1$, and $\lambda = 0.1$, depicts rational soliton, which is strongly localized in space and decays algebraically. These solutions describe localized excitations in physical systems such as magneto-optic waveguides and plasmas, where energy is limited to a small region. The depth of the notch is controlled by amplitude parameters (e.g., b_1) and nonlinear factors, while its width is set by the dispersion d_1. Noise intensity ϵ affects the background

and the notch depth. Moderate noise causes slow relaxation and reduces the contrast, while a very small ϵ keeps the dark soliton almost unchanged.

Figure 4 represents the bifurcation scenario derived from the dynamical system. The diagram illustrates the transition of equilibrium states, demonstrating a loss of stability and a qualitative structural change in response to parameter variations. Higher dispersion d_1 or large nonlinear coefficients displaced the bifurcation threshold. ω_0 does not affect the bifurcation threshold. At small values, noise intensity ϵ stabilizes the system and delays bifurcation, whereas large ϵ speeds up the loss of stability.

Figures 5–7 illustrate the chaotic dynamics of the coupled system. The time series, phase portraits, and chaotic attractors reveal irregular oscillations and sensitivity to initial conditions. These plots emphasize the parametric dependence of the chaotic waveform under changes in dispersion, soliton velocity, and nonlinearity. Variations in soliton velocity ω_0 modulate the oscillation frequency, dispersion d_1 enlarges the chaotic envelope, and nonlinear coefficients (k_1, m_1) determine the intensity of fluctuation strength. The stochastic parameter ϵ modulates dynamics: moderate levels (e.g., $\epsilon = 0.5$) yield partial stabilization with smoother attractors, while larger levels ($\epsilon > 1$) amplify the fluctuations, expand attractor basins, and intensify chaotic divergences. Overall, these figures demonstrate the coexistence of deterministic chaos and stochastic effects within the nonlinear wave system.

Figures 9 and 10 depict the Lyapunov exponents of the coupled nonlinear system, offering a quantitative measure of stability and chaotic behavior. Negative values of the Lyapunov exponents denote stable soliton propagation, whereas positive values signify chaotic behavior with sensitivity to initial conditions. The parameter dependence of the maximal Lyapunov exponent clearly indicates a transition between stability and chaos. An increase in the dispersion coefficients d_1 broadens the domain of stability, whereas stronger nonlinear effects diminish it. The soliton velocity ω_0 changes the positions of the transition points without modifying the intrinsic qualitative nature of the dynamics. The stochastic parameter ϵ exerts a strong influence on the Lyapunov spectrum: intermediate noise ($\epsilon = 0.5$) lowers the maximum Lyapunov spectrum, indicating noise-induced stabilization, while higher levels ($\epsilon > 1$) amplify the exponent, reinforcing instability and accelerating the onset of chaotic dynamics.

Figures 11 and 12 analyze the system's susceptibility to variation in initial states and perturbations of control parameters. The results highlight that even small changes in initial states or system parameters yield significantly different solution trajectories, evidencing the inherent chaotic and stochastic dynamics of the nonlinear model. Figure 11 demonstrates trajectory divergence under small perturbations in the initial amplitude, representing a canonical signature of deterministic chaos. Figure 12 depicts the pronounced sensitivity of solution profiles to soliton velocity ω_0, wherein even minimal variations generate substantial deviations. Figure 13 examines the stochastic effects, demonstrating that under moderate noise ($\epsilon = 0.5$), the divergence between initially close solutions slows down (indicating noise-induced stabilization), whereas at higher noise levels ($\epsilon > 1$), divergence accelerates, increasing instability.

5.1. Implications of chaotic dynamics in magneto-optic waveguides

Chaotic behavior in magneto-optic waveguides, evidenced by positive Lyapunov exponents, indicates that infinitesimal variations in initial conditions amplify exponentially over time. Such sensitivity suggests that minor perturbations in light amplitude, phase, or polarization may cause unpredictable alterations in the output, including amplitude fluctuations, waveform distortion, or timing

jitter.

- **Signal integrity:** The exponential divergence in chaotic trajectories may reduce signal fidelity, presenting significant challenges in high-speed or long-distance communications.
- **System design:** Active feedback or adaptive stabilization may be necessary to suppress chaos and ensure a stable signal propagation, potentially through real-time modulation of the applied magnetic field or waveguide refractive index.
- **Exploitation potential:** Conversely, the controlled utilization of chaos may enable applications such as optical communication or random number generation, leveraging sensitivity to initial conditions for unpredictability and encryption strength.

6. Conclusions

In this study, we systematically analyzed dynamics in coupled magneto-optic waveguides via the generalized Arnous method for stochastic Schrödinger–Hirota equation. NLPDE was converted into PDE through traveling wave transformation. After that, the construction and implementation of the generalized Arnous method applied to the proposed Eq (1.1) demonstrated the applicability of our model. We successfully constructed a wide range of solitary wave solutions, including dark, bright, and kink structures. The obtained solutions, including logarithmic, exponential, trigonometric, and multi-wave structures, show rich nonlinear behavior and reveal that the system can exhibit chaotic dynamics, as confirmed by positive Lyapunov exponents. This reflects a strong sensitivity to initial conditions, showing that even small perturbations in input amplitude, phase, or polarization may lead to significant signal distortion. The exact solutions obtained in this study exhibit distinct physical characteristics. The bright and dark soliton solutions represent stable localized pulses in optical fibers, where dispersion and nonlinearity counterbalance each other. Through stability and phase-space analysis, we showed that small perturbations preserve the soliton structure, while larger parameter variations may trigger quasi-periodic or chaotic responses. These properties demonstrate that the derived solutions are not only mathematically valid but also physically relevant for modeling nonlinear wave propagation in realistic optical systems. Despite these findings, the present study has certain limitations. Only the nonlinear term with n=1 has been considered, and higher-order nonlinearities, multi-dimensional interactions, and parameter variability effects have not been explored. Consequently, the current analysis is restricted to a specific parameter regime, and the effect of multiple interactions among multiple solitons or higher-order effects remains to be investigated. Future work should extend the analysis to higher-order nonlinear terms and multi-dimensional soliton interactions, such as lump soliton collisions and fusion. Such studies would provide deeper insight into the practical capabilities and limitations of magneto-optic waveguides in real-world optical systems.

Author contributions

Khizar Farooq: Formal analysis, Methodology, Supervision, Writing–review and editing; Aljethi Reem Abdullah: Validation, Funding, Project administration; Ejaz Hussain: Software, Methodology, Writing–review and editing; Muhammad Amin S. Murad: Investigation, Supervision.

Use of Generative-AI tools declaration

The authors declare they have not used Artificial Intelligence (AI) tools in the creation of this article.

Funding

This work was funded by the Deanship of Scientific Research at Imam Mohammad Ibn Saud Islamic University (IMSIU) (grant number IMSIU-DDRSP2502).

Conflict of interest

The authors declare no conflicts of interest to report regarding the present study.

Data availability

The data that support the findings of this study are available from the corresponding author upon reasonable request.

References

1. A. Sommerfeld, *Partial differential equations in physics*, Academic Press, 1949. https://doi.org/10.1016/B978-0-12-654658-3.X5001-0
2. W. F. Ames, *Nonlinear partial differential equations in engineering*, Academic Press, 1965.
3. S. M. R. Islam, K. Khan, M. A. Akbar, Optical soliton solutions, bifurcation, and stability analysis of the Chen-Lee-Liu model, *Results Phys.*, **51** (2023), 106620. https://doi.org/10.1016/j.rinp.2023.106620
4. R. A. M. Attia, Y. Xia, X. Zhang, M. M. A. Khater, Analytical and numerical investigation of soliton wave solutions in the fifth-order KdV equation within the KdV-kP framework, *Results Phys.*, **51** (2023), 106646. https://doi.org/10.1016/j.rinp.2023.106646
5. M. M. A. Khater, Physics of crystal lattices and plasma; analytical and numerical simulations of the Gilson–Pickering equation, *Results Phys.*, **44** (2023), 106193. https://doi.org/10.1016/j.rinp.2022.106193
6. E. Hussain, A. H. Tedjani, K. Farooq, Beenish, Modeling and exploration of localized wave phenomena in optical fibers using the generalized Kundu–Eckhaus equation for femtosecond pulse transmission, *Axioms*, **14** (2025), 513. https://doi.org/10.3390/axioms14070513
7. M. M. A. Khater, Abundant and accurate computational wave structures of the nonlinear fractional biological population model, *Int. J. Mod. Phys. B*, **37** (2023), 2350176. https://doi.org/10.1142/S021797922350176X
8. G. Karamali, M. Dehghan, M. Abbaszadeh, Numerical solution of a time-fractional PDE in the electroanalytical chemistry by a local meshless method, *Eng. Comput.-Germany*, **35** (2019), 87–100. https://doi.org/10.1007/s00366-018-0585-7

9. E. Zauderer, *Partial differential equations of applied mathematics*, John Wiley & Sons, 2011. https://doi.org/10.1002/9781118033302

10. N. Tufillaro, An experimental approach to nonlinear dynamics and chaos, ScienceOpen Preprints, 2024.

11. M. A. Chowdhury, M. M. Miah, M. M. Rasid, S. Rehman, J. R. M. Borhan, A.-M. Wazwaz, et al., Further quality analytical investigation on soliton solutions of some nonlinear PDEs with analyses: Bifurcation, sensitivity, and chaotic phenomena, *Alex. Eng. J.*, **103** (2024), 74–87. https://doi.org/10.1016/j.aej.2024.05.096

12. M. A. Zidan, Y. Jeong, J. Lee, B. Chen, S. Huang, M. J. Kushner, et al., A general memristor-based partial differential equation solver, *Nat. Electron.*, **1** (2018), 411–420. https://doi.org/10.1038/s41928-018-0100-6

13. F. Gaitan, Finding solutions of the Navier-Stokes equations through quantum computing—recent progress, a generalization, and next steps forward, *Adv. Quantum Technol.*, **4** (2021), 2100055. https://doi.org/10.1002/qute.202100055

14. M. A. E. Abdelrahman, E. H. M. Zahran, M. M. A. Khater, The Exp $(-\varphi(\xi))$-expansion method and its application for solving nonlinear evolution equations, *International Journal of Modern Nonlinear Theory and Application*, **4** (2015), 37.

15. S. A. El-Wakil, M. A. Abdou, The extended mapping method and its applications for nonlinear evolution equations, *Phys. Lett. A*, **358** (2006), 275–282. https://doi.org/10.1016/j.physleta.2006.05.040

16. S. M. R. Islam, Bifurcation analysis and exact wave solutions of the nano-ionic currents equation: via two analytical techniques, *Results Phys.*, **58** (2024), 107536. https://doi.org/10.1016/j.rinp.2024.107536

17. J.-H. He, Homotopy perturbation method: a new nonlinear analytical technique, *Appl. Math. Comput.*, **135** (2003), 73–79. https://doi.org/10.1016/S0096-3003(01)00312-5

18. C. Gu, H. Hu, Z. Zhou, *Darboux transformations in integrable systems: theory and their applications to geometry*, Dordrecht: Springer, 2004. https://doi.org/10.1007/1-4020-3088-6

19. M. S. Islam, K. Khan, A. H. Arnous, Generalized Kudryashov method for solving some (3+1)-dimensional nonlinear evolution equations, *New Trends in Mathematical Sciences*, **3** (2015), 46–57.

20. Y. Gurefe, E. Misirli, A. Sonmezoglu, M. Ekici, Extended trial equation method to generalized nonlinear partial differential equations, *Appl. Math. Comput.*, **219** (2013), 5253–5260. https://doi.org/10.1016/j.amc.2012.11.046

21. J. Hietarinta, Introduction to the Hirota bilinear method, In: *Integrability of nonlinear systems*, Berlin, Heidelberg: Springer, 2007, 95–103. https://doi.org/10.1007/BFb0113694

22. Z. Li, E. Hussain, Qualitative analysis and traveling wave solutions of a (3+1)-dimensional generalized nonlinear Konopelchenko–Dubrovsky–Kaup–Kupershmidt system, *Fractal Fract.*, **9** (2025), 285. https://doi.org/10.3390/fractalfract9050285

23. Z. Yan, The extended Jacobian elliptic function expansion method and its application in the generalized Hirota–Satsuma coupled KdV system, *Chaos Soliton. Fract.*, **15** (2003), 575–583. https://doi.org/10.1016/S0960-0779(02)00145-5

24. S. M. Mirhosseini-Alizamini, H. Rezazadeh, M. Eslami, M. Mirzazadeh, A. Korkmaz, New extended direct algebraic method for the Tzitzica type evolution equations arising in nonlinear optics, *Comput. Methods Differ. Equ.*, **8** (2020), 28–53.

25. K. Farooq, E. Hussain, H. A. Abujabal, F. S. Alshammari, Propagation of nonlinear dispersive waves in shallow water and acoustic media in the framework of integrable Schwarz–Korteweg–de Vries equation, *AIMS Math.*, **10** (2025), 17543–17566. https://doi.org/10.3934/math.2025784

26. S. A. El-Wakil, M. A. Abdou, The extended Fan sub-equation method and its applications for a class of nonlinear evolution equations, *Chaos Soliton. Fract.*, **36** (2008), 343–353. https://doi.org/10.1016/j.chaos.2006.06.065

27. G. L. Lamb Jr., Bäcklund transformations for certain nonlinear evolution equations, *J. Math. Phys.*, **15** (1974), 2157–2165. https://doi.org/10.1063/1.1666595

28. Z. Li, Optical solutions of the nonlinear Kodama equation with the M-truncated derivative via the extended $(G'/G)-$expansion method, *Fractal Fract.*, **9** (2025), 300. https://doi.org/10.3390/fractalfract9050300

29. M. A. Abdou, A generalized auxiliary equation method and its applications, *Nonlinear Dyn.*, **52** (2008), 95–102. https://doi.org/10.1007/s11071-007-9261-y

30. M. E. Islam, M. M. Hossain, K. M. Helal, U. S. Basak, R. C. Bhowmik, M. A. Akbar, Solitary wave analysis of the Kadomtsev–Petviashvili model in mathematical physics, *Arab Journal of Basic and Applied Sciences*, **30** (2023), 329–340. https://doi.org/10.1080/25765299.2023.2216536

31. N. A. Kudryashov, Method for finding highly dispersive optical solitons of nonlinear differential equations, *Optik*, **206** (2020), 163550. https://doi.org/10.1016/j.ijleo.2019.163550

32. K. Farooq, E. Hussain, U. Younas, H. Mukalazi, T. M. Khalaf, A. Mutlib, et al., Exploring the wave's structures to the nonlinear coupled system arising in surface geometry, *Sci. Rep.*, **15** (2025), 11624. https://doi.org/10.1038/s41598-024-84657-w

33. J. Skipp, J. Laurie, S. Nazarenko, Hamiltonian derivation of the point vortex model from the two-dimensional nonlinear Schrödinger equation, *Phys. Rev. E*, **107** (2023), 025107. https://doi.org/10.1103/PhysRevE.107.025107

34. M. A. S. Murad, F. S. Alshammari, M. S. Salih, K. Farooq, Optical soliton structures in the nonlinear conformable Schrödinger equation with quadratic–cubic nonlinearity, *Nonlinear Dyn.*, in press. https://doi.org/10.1007/s11071-025-11775-z

35. V. P. Shyaman, A. Sreelakshmi, A. Awasthi, An adaptive tailored finite point method for the generalized Burgers' equations, *J. Comput. Sci.*, **62** (2022), 101744. https://doi.org/10.1016/j.jocs.2022.101744

36. T. Alotaibi, A. Althobaiti, Exact solutions of the nonlinear modified Benjamin-Bona-Mahony equation by an analytical method, *Fractal Fract.*, **6** (2022), 399. https://doi.org/10.3390/fractalfract6070399

37. B. A. Alwan, M. A. Bakar, W. A. Faridi, A. Turcu, A. Akgül, M. Sallah, The propagating exact solitary waves formation of generalized Calogero–Bogoyavlenskii–Schiff equation with robust computational approaches, *Fractal Fract.*, **7** (2023), 191. https://doi.org/10.3390/fractalfract7020191

38. S. Singh, S. S. Ray, Integrability and new periodic, kink-antikink and complex optical soliton solutions of (3+1)-dimensional variable coefficient DJKM equation for the propagation of nonlinear dispersive waves in inhomogeneous media, *Chaos Soliton. Fract.*, **168** (2023), 113184. https://doi.org/10.1016/j.chaos.2023.113184

39. M. M. A. Khater, Computational simulations of propagation of a tsunami wave across the ocean, *Chaos Soliton. Fract.*, **174** (2023), 113806. https://doi.org/10.1016/j.chaos.2023.113806

40. K. Farooq, F. S. Alshammari, Z. Li, E. Hussain, Soliton dynamics and stability in the Boussinesq equation for shallow water applications, *Front. Phys.*, **13** (2025), 1637491. https://doi.org/10.3389/fphy.2025.1637491

41. W. A. Faridi, S. A. AlQahtani, The explicit power series solution formation and computation of Lie point infinitesimals generators: Lie symmetry approach, *Phys. Scr.*, **98** (2023), 125249. https://doi.org/10.1088/1402-4896/ad0948

42. Y. Zhao, C. Xu, Y. Xu, J. Lin, Y. Pang, Z. Liu, et al., Mathematical exploration on control of bifurcation for a 3D predator–prey model with delay, *AIMS Math.*, **9** (2024), 29883–29915. https://doi.org/10.3934/math.20241445

43. Q. Cui, C. Xu, Y. Xu, W. Ou, Y. Pang, Z. Liu, et al., Bifurcation and controller design of 5D BAM neural networks with time delay, *Int. J. Numer. Model. Electron. Netw. Devices Fields*, **37** (2024), e3316. https://doi.org/10.1002/jnm.3316

44. E. M. E. Zayed, R. M. A. Shohib, M. E. M. Alngar, Dispersive optical solitons in magneto-optic waveguides with stochastic generalized Schrödinger–Hirota equation, *Optik*, **271** (2022), 170069. https://doi.org/10.1016/j.ijleo.2022.170069

45. E. M. E. Zayed, R. M. A. Shohib, M. E. M. Alngar, A. Biswas, L. Moraru, S. Khan, et al., Dispersive optical solitons with Schrödinger–Hirota model having multiplicative white noise via Itô calculus, *Phys. Lett. A*, **445** (2022), 128268. https://doi.org/10.1016/j.physleta.2022.128268

46. L. Tang, Optical solitons perturbation and traveling wave solutions in magneto-optic waveguides with the generalized stochastic Schrödinger–Hirota equation, *Opt. Quant. Electron.*, **56** (2024), 773. https://doi.org/10.1007/s11082-024-06669-0

47. H. Cakicioglu, M. Ozisik, A. Secer, M. Bayram, Optical soliton solutions of Schrödinger–Hirota equation with parabolic law nonlinearity via generalized Kudryashov algorithm, *Opt. Quant. Electron.*, **55** (2023), 407. https://doi.org/10.1007/s11082-023-04634-x

48. S. Kumar, I. Hamid, M. A. Abdou, Dynamic frameworks of optical soliton solutions and soliton-like formations to Schrödinger–Hirota equation with parabolic law non-linearity using a highly efficient approach, *Opt. Quant. Electron.*, **55** (2023), 1261. https://doi.org/10.1007/s11082-023-05461-w

49. A. Biswas, M. Mirzazadeh, M. Eslami, Dispersive dark optical soliton with Schrödinger–Hirota equation by G'/G-expansion approach in power law medium, *Optik*, **125** (2014), 4215–4218. https://doi.org/10.1016/j.ijleo.2014.03.039

50. B. Kilic, M. Inc, Optical solitons for the Schrödinger–Hirota equation with power law nonlinearity by the Bäcklund transformation, *Optik*, **138** (2017), 64–67. https://doi.org/10.1016/j.ijleo.2017.03.017

51. T. Han, Y. Liang, W. Fan, Dynamics and soliton solutions of the perturbed Schrödinger–Hirota equation with cubic–quintic–septic nonlinearity in dispersive media, *AIMS Math.*, **10** (2025), 754–776. https://doi.org/10.3934/math.2025035

52. M. Khaliq, S. Ahmad, A. Ullah, H. Ahmad, S. Saifullah, T. A. Nofal, New waves solutions of the (2+1)-dimensional generalized Hirota–Satsuma–Ito equation using a novel expansion method, *Results Phys.*, **50** (2023), 106450. https://doi.org/10.1016/j.rinp.2023.106450

53. T. Han, H. Rezazadeh, M. U. Rahman, High-order solitary waves, fission, hybrid waves and interaction solutions in the nonlinear dissipative (2+1)-dimensional Zabolotskaya–Khokhlov model, *Phys. Scr.*, **99** (2024), 115212. https://doi.org/10.1088/1402-4896/ad7f04

54. K. Farooq, A. H. Tedjani, Z. Li, E. Hussain, Soliton dynamics of the nonlinear Kodama equation with M-truncated derivative via two innovative schemes: the generalized Arnous method and the Kudryashov method, *Fractal Fract.*, **9** (2025), 436. https://doi.org/10.3390/fractalfract9070436

55. Beenish, H. Kurkcu, M. B. Riaz, M. Imran, A. Jhangeer, Lie analysis and nonlinear propagating waves of the (3+1)-dimensional generalized Boiti–Leon–Manna–Pempinelli equation, *Alex. Eng. J.*, **80** (2023), 475–486. https://doi.org/10.1016/j.aej.2023.08.067

56. Z. Li, J. Lyu, E. Hussain, Bifurcation, chaotic behaviors and solitary wave solutions for the fractional Twin-Core couplers with Kerr law non-linearity, *Sci. Rep.*, **14** (2024), 22616. https://doi.org/10.1038/s41598-024-74044-w

57. S. A. A. Shah, E. Hussain, W.-X. Ma, Z. Li, A. E. Ragab, T. M. Khalaf, Qualitative analysis and new variety of solitons profiles for the (1+1)-dimensional modified equal width equation, *Chaos Soliton. Fract.*, **187** (2024), 115353. https://doi.org/10.1016/j.chaos.2024.115353

58. Z. U. Rehman, Z. Hussain, Z. Li, T. Abbas, I. Tlili, Bifurcation analysis and multi-stability of chirped form optical solitons with phase portrait, *Results Eng.*, **21** (2024), 101861. https://doi.org/10.1016/j.rineng.2024.101861

59. A. Jhangeer, Beenish, A. M. Talafha, A. R. Ansari, M. Imran, Analytical and dynamical analysis of nonlinear Riemann wave equation in plasma systems, *Arab Journal of Basic and Applied Sciences*, **31** (2024), 536–553.

AIMS Press